Journal of Geochemical Exploration 287 (2026) 108060

Contents lists available at ScienceDirect

Journal of Geochemical Exploration

journal homepage: www.elsevier.com/locate/gexplo

Insights into the mineralogy and distribution of Co, Ni, As and Bi in the sediment-hosted polymetallic ores of the Kupferschiefer in Lusatia, Germany

Zahra Nourizenouz [a,*], Max Frenzel [b], Bradley Martin Guy [a], Aratz Beranoaguirre [c], Jens Gutzmer [a]

[a] Helmholtz-Zentrum Dresden-Rossendorf, Helmholtz Institute Freiberg for Resource Technology, Freiberg, Germany
[b] King Abdullah University of Science and Technology, Physical Science and Engineering Division, Thuwal, Saudi Arabia
[c] Karlsruhe Institute for Technology, Chair of Economic Geology and Geochemistry, Karlsruhe, Germany

ARTICLE INFO

Keywords:
Kupferschiefer
By-products
LA-ICP-MS
metal deportment

ABSTRACT

The Kupferschiefer ores of Central Europe have long served as an important source of Cu and Ag, but have also yielded a number of important by-product metals, including Pb, Zn, Co, Ni, Ge, Re, and Au. However, little is known about the mineralogy and distribution of such by-product metals. The present study provides a comprehensive assessment for the mineralogy and distribution of potential value-adding by-products (Co and Ni) and deleterious elements (As and Bi) in drill-cores from the Spremberg-Graustein-Schleife prospect in Lusatia, Germany. Detailed mineralogical investigations were conducted using scanning electron microscope-based automated mineralogy to identify and quantify the abundance of minerals hosting Co, Ni, As, and Bi. Major sulfide minerals were analyzed by laser ablation-inductively coupled plasma-mass spectrometry to constrain their trace element compositions and to assess their contribution to the bulk content of the four target elements. The results show that the bulk of Co and Ni is hosted in major sulfides, discrete Co and Ni minerals, as well as gangue minerals. In the copper-mineralized samples, most of the recoverable Co and Ni occur as fine cobaltite – gersdorffite inclusions within Cu-sulfides. The two deleterious elements illustrate a very different distribution. Arsenic occurs primarily in cobaltite – gersdorffite and pyrite, whereas Bi is mainly incorporated into Cu-sulfides. The results have important implications for the recovery of these four target elements during industrial mineral processing. Recovery of Ni and Co will be limited by their deportment to gangue minerals (including pyrite). Bismuth, as well as As, will effectively report to the Cu concentrate. Because of low bulk concentrations in the ore, Bi contents in the copper concentrate can be expected to remain below smelter penalty levels. This is markedly different for As contents in the Cu concentrate that may, in fact, approach smelter penalty levels.

1. Introduction

The shift towards renewable energies, electrification, and digitalization gives rise to a rapid increase in global demand for raw materials (IEA, 2024). Concerns relating to supply security are escalating, particularly in many highly industrialized nations that depend largely on raw material imports (European Commission, 2023; U.S. Department of Energy, 2023). While risks in the major commodity markets, such as Cu and Al, are well constrained, many minor metals that are essential to modern society are primarily recovered as by-products with small annual production volumes and complex commodity supply chains that are limited to a small number of suppliers and traders (Nassar et al., 2015). The lack of information can begin as early as the exploration phase, where potential by-products are typically evaluated only through geochemical assay campaigns with no evaluation of their mineralogical distribution. Thus, their economic potential is frequently overlooked in both early-stage exploration and subsequent feasibility studies, which ultimately inform processing route decisions. The potential to recover these by-products is, however, usually dependent on the beneficiation route chosen for the major products (Greffe et al., 2024).

Despite the growing importance of by-product metals, quantitative studies on their mineralogical deportment and distribution within ore

* Corresponding author.
E-mail address: z.nourizenouz@hzdr.de (Z. Nourizenouz).

https://doi.org/10.1016/j.gexplo.2026.108060
Received 30 November 2025; Received in revised form 26 March 2026; Accepted 30 March 2026
Available online 4 April 2026

deposits continue to be underrepresented within scientific literature (Mudd et al., 2017; Frenzel et al., 2019). This is largely due to the inherent complexity and costs associated with detailed characterization studies, which require the evaluation of a representative suite of samples across an ore deposit and the integration of data from multiple analytical techniques. Representative samples are typically analyzed using scanning electron microscopy (SEM)-based automated mineralogy (AM) to identify host minerals for major and minor elements, with results validated through bulk chemical assays (Goodall et al., 2005; Coetzee et al., 2011). Further analysis of the host minerals using electron probe microanalyzer (EPMA) and laser ablation-inductively coupled plasma mass-spectrometry (LA-ICP-MS) is required to determine the deportment for minor and trace elements. While such quantitative studies are more common for noble metals (e.g., Chryssoulis and Cabri, 1990; Butcher et al., 2000; Goodall, 2008; Cabri et al., 2009), they remain scarce for non-precious and by-product metals (e.g., Frenzel et al., 2019; Kelvin et al., 2022; Zhang et al., 2024). This lack of quantitative assessment is particularly notable for well-known polymetallic ore types, despite the insights it could provide into potential by-product supplies (Frenzel et al., 2015, 2017).

The sediment-hosted stratabound copper (SSC) deposits of the Kupferschiefer in Central Europe are a prime example of a polymetallic ore type. Not only are these deposits a significant source of Cu and Ag, they also contain elevated concentrations of several other metals, including Pb, Zn, Co, Ni, Ge, Re, and Au (Borg et al., 2012; Vind and Tamm, 2021; Kopp, 2022). While the industrial exploitation of the Kupferschiefer is currently limited to Poland, there is extensive exploration taking place in both Poland and Germany, including the Spremberg-Graustein-Schleife prospect in Brandenburg and Saxony, which is currently owned by KSL Kupferschiefer Lausitz GmbH.

The polymetallic character of the Kupferschiefer ores is aptly illustrated by current operations in Poland (managed by KGHM Polska Miedź S.A.), where by-product metals, such as Au, Pb, Re, and Ni, are recovered in addition to Cu and Ag (KGHMa, 2025). In the Mansfeld and Sangerhausen regions in central Germany, prior to the closure of the mining operations in 1990, more than 20 metals were recovered either continuously or intermittently, depending on their concentrations in the bulk ore (Klette, 2003; Spilker, 2010). The approach in central Germany involved smelting the entire organic-rich marl/shale unit of the Kupferschiefer, with its finely disseminated sulfide mineralization, directly in so-called shaft furnaces to produce Cu matte that was then refined further. This approach was feasible under the economic conditions prevailing at the time. In present-day operations in Poland, in contrast, a Cu-rich sulfide concentrate is first produced by froth flotation, and then smelted using flash smelting technology or, alternatively, shaft furnace technology to yield copper matte. This matte is subsequently converted into blister copper and further refined to high-purity cathode copper (KGHMb, 2025).

To assess the possibilities of recovering Co and Ni as potential by-products from Cu-rich mineral concentrates obtained from Kupferschiefer-type ores, it is crucial to quantitatively assess the deportment of these two metals. It is equally important to quantify the deportment of deleterious elements, such as As and Bi, which pose environmental concerns, impair product quality, and increase processing costs (Fountain, 2013). Little is currently known about the distribution of Bi in Kupferschiefer ores. Arsenic, on the other hand, is a stoichiometric constituent in several of the Cu ore minerals in Kupferschiefer ores, including tennantite ($Cu_{12}As_4S_{13}$) and enargite (Cu_3AsS_4), but may also occur as a trace constituent in minerals like pyrite. Tennantite and enargite exhibit comparable flotation characteristics to copper sulfides and will thus report to the concentrate. Arsenic is volatilized during the Cu smelting process, entering the furnace off-gases and later condensing in flue dusts, leading to significant emission and contamination risks (Long et al., 2012). Bismuth, in contrast, is highly insoluble in copper metal, where even trace amounts can cause brittleness, requiring further refining (Duscher et al., 2004). Assessing the deportments of As and Bi, alongside Co and Ni, is therefore important to optimize processing efficiency and product quality, and to minimize environmental impacts and costs.

This study investigates the mineralogy and distribution of Co, Ni, As, and Bi in samples from exploration drill-cores of the Spremberg-Graustein-Schleife Kupferschiefer prospect in Lusatia, Germany. It builds on previous work, in which the deportment of Ag in the same sample suite was investigated (Nourizenouz et al., 2026). Comprehensive mineralogical analyses using SEM-based AM were conducted to identify and quantify the modal abundances of the principal Co-, Ni-, As-, and Bi-containing minerals. Subsequently, mineral chemical analyses, including LA-ICP-MS and EPMA, were carried out on major base-metal sulfides, such as chalcocite-group minerals, covellite, bornite, and chalcopyrite, as well as sphalerite, galena, and pyrite, to quantify the distribution of Co, Ni, As, and Bi between these common sulfide minerals. This knowledge is then used to place constraints on the recovery of Co and Ni as by-products to a Cu concentrate and to predict whether concentrations of As and Bi in the concentrate exceed threshold levels and incur smelter penalties.

2. Geological setting

The Kupferschiefer ore deposits are hosted within the Southern Permian Basin (SPB), an extensive intracontinental basin that stretches from England across the North Sea, northern Germany, and Poland to the Baltic States (Ziegler, 1990). This basin formed during the late Carboniferous period (~300 Ma), following the Variscan Orogeny, and developed as a successor to the Variscan foredeep along the northern margin of the orogenic belt (van Wees et al., 2000). The formation of the SPB was driven by post-orogenic tectonics, characterized by strike-slip faulting and the formation of pull-apart basins (Ziegler, 1990). Bimodal volcanism was initially widespread; volcanic rocks and interbedded fluvial and lacustrine sedimentary strata constitute the Permian Lower Rotliegend Subgroup (Geißler et al., 2008). Subsequent crustal uplift and erosion, marked by the Saalian Unconformity, were followed by thermal subsidence and renewed sedimentation in arid environments (Glennie, 1997). This latter phase led to the deposition of the Upper Rotliegend Subgroup, characterized by extensive continental evaporite deposits and sedimentary features typical of desert conditions in the SPB (Stollhofen et al., 2008).

During the late Permian (~258 Ma), the shallow continental Zechstein Sea formed following rapid marine transgression across much of the SPB. This resulted in the deposition of a thin, carbonaceous black marl/shale unit, the so-called Kupferschiefer (T1) at the base of the Zechstein Group that conformably overlies the Rotliegend Group sandstones (S1) with a sharp contact (Glennie, 1997). The Zechstein Group is subdivided into several cycles, reflecting progressive evaporation and chemical precipitation that filled the SPB. Evaporation cycles typically begin with the deposition of marls or limestones, followed by evaporites, including gypsum/anhydrite and halite (Tucker, 1991; Strohmenger et al., 1996; Kaiser et al., 2003). Zechstein Limestone (Ca1), overlying the T1, is the first carbonate-rich unit deposited during the first evaporitic cycle.

The sulfide mineralization in the Kupferschiefer ores reflects a complex, multi-stage paragenetic sequence, with different textural styles of sulfide mineralization, including fine disseminations, crosscutting/bedding-parallel veins, and replacement of carbonate cements, fossils, and detrital clasts (Borg et al., 2012). High-grade base metal mineralization is distinctly zoned, both laterally and vertically, and is genetically associated with a prominent post-depositional oxidation front known as “Rote Fäule”. Immediately adjacent to the Rote Fäule oxidation front, a Cu-Ag mineralization zone is developed, consisting of chalcocite, covellite, bornite, and chalcopyrite. Locally, a thin zone of precious metal enrichment (e.g., Au, Pt, Pd) has been described along the immediate redox boundary (Piestrzyński et al., 2002). With increasing distance to the oxidation front, Cu-Ag mineralization is followed by Pb-

Zn (galena and sphalerite) and Fe (pyrite) mineralization. The latter carries only negligible base metal concentrations (Borg et al., 2012).

The Spremberg-Graustein-Schleife Kupferschiefer prospect in Lusatia, eastern Germany, is situated between the historical German mining districts of Mansfeld and Sangerhausen and the active mining operations in Southwest Poland (Fig. 1a). Targeted exploration was carried out from 1954 to 1980 and restarted in 2009 by KSL. The prospect extends over a total area of 15 km by 3.5 km, and consists of two disjointed orebodies, called the Spremberg and Graustein fields. These are separated by the Türkendorfer Graben, a prominent NE–SW-striking graben structure (Fig. 1b). The bulk of these orebodies is located in the state of Brandenburg. The term "Schleife" denotes the southeasterly extension of the Graustein field into the jurisdiction of the Free State of Saxony. The Cu-Ag mineralization lies at a depth of 800 to 1500 m, with an average thickness of 2.4 m. Indicated and inferred resources consist of 115.2 Mt. at 1.47% Cu and 24.1 g/t Ag, and 14.5 Mt. at 1.46% Cu and 29.9 g/t Ag, respectively (KSL report, 2021).

3. Material and methods

3.1. Sampling and sample preparation

For this study, 53 samples were collected from three exploration drill-cores (131, 133, and 136), all drilled in 2009 by KSL (Fig. 1b). Drill-cores 131 and 133 are situated in the Graustein area, whereas drill-core 136 is located within the Türkendorfer Graben (Fig. 1c). Each of the three drill-cores intersected the S1, T1, and Ca1 units. Regarding mineralization in the T1 unit, drill-cores 131 and 133 intersected Cu-Ag mineralization, whereas drill-core 136 intersected Pb-Zn mineralization. Notably, drill-core 133 shows evidence of the Rote Fäule oxidation front at the base of the T1 unit (Fig. A1). Slab samples (~ 2 cm thick and ~ 4 cm wide) were cut from the drill-cores using an NTT Coresaw at the Helmholtz Institute Freiberg for Resource Technology (HIF). The lengths of the slab samples correspond to the lengths of the sampling intervals previously defined and assayed by KSL (see ESM-2 for details).

The sample preparation process consisted of several steps, which involved crushing, splitting, and compositing (see Nourizenouz et al., 2026). Samples were initially crushed in stages to 100% passing 500 μm and split into representative aliquots using a laboratory rotary splitter. To improve representativeness for the scale of mining and reduce analytical costs, the 53 samples were composited into 19 composite samples. Compositing was performed within individual lithological units. Base-metal assay data (Cu, Pb, and Zn) were used as the geochemical criteria guiding aggregation. While this approach may smooth small-scale whole rock geochemical and mineralogical heterogeneity, it provides representative bulk compositions at a scale relevant to mining and processing operations.

One aliquot of each composite sample was reserved for mineral chemical analysis by EPMA and LA-ICP-MS. A second aliquot was milled to 95% passing 100 μm for SEM-based AM, while a third aliquot was milled to 100% passing 63 μm for bulk geochemical analysis. For SEM-based AM, polished epoxy grain mounts (30 mm diameter) were prepared by embedding the milled material within a mixture of epoxy resin, graphite powder, and 10 wt% iodine. The addition of iodine helps to differentiate organic carbon from the epoxy resin in back-scattered electron (BSE) images (Rahfeld and Gutzmer, 2017). To minimize bias from gravitational settling, the mounts were sliced vertically, rotated 90°, and remounted in 30 mm epoxy resin (Heinig et al., 2015).

Heavy liquid separation (HLS) was carried out on the crushed material (100% passing 500 μm) to upgrade the sulfide content for point analysis by LA-ICP-MS and EPMA. Sodium polytungstate salt (SPT; $3Na_2WO_4{\cdot}9WO_3{\cdot}H_2O$) was dissolved in water to achieve a density of 3.1 g/cm^3. The resulting sink fractions were washed with distilled water, dried in the oven overnight at 48 °C, and then embedded in epoxy resin. These epoxy grain mounts were also sliced vertically, rotated by 90°, and remounted in epoxy resin blocks (25 mm diameter). Due to low mass recoveries in the sink fractions, several samples were prepared without rotation and remounting (samples 131–1, 131–8, 133–5, and 133–6).

3.2. Bulk geochemistry

In addition to the geochemical assay data provided by KSL for the initial 53 intervals, in-house XRF analyses were conducted on the newly sampled material with the same sampling intervals as KSL to validate sampling and sample preparation. Furthermore, the finely milled aliquots (100% passing 63 μm) of the 19 composite samples were analyzed at Actlabs in Canada using the Ultratrace-3 multi-element analytical package (Actlabs, 2023). This program involves four-acid digestion ($HCl\text{-}HNO_3\text{-}HClO_4\text{-}HF$), followed by ICP-OES and ICP-MS analyses. The concentration of As was quantified by instrumental neutron activation analysis (INAA), since As is susceptible to volatilization during acid digestion. The total organic carbon content was determined by infrared spectroscopy (IR). To assess analytical precision, four duplicates of the drill-core composite samples were included. To evaluate analytical accuracy, four OREAS certified reference materials (CRMs) were submitted as unknowns: three from sediment-hosted Cu deposits (OREAS 554, 902, and 993) and one from a porphyry Cu-Au deposit (OREAS 504d).

3.3. Mineralogy

Reflected- and transmitted-light microscopy were carried out on all of the grain mounts prepared for this study using a Carl Zeiss Axio Imager Z2m, equipped with an AxioCam MRc camera at the HIF. In addition, several polished thin sections provided by KSL were examined using optical microscopy. These observations were used to obtain an overview of the ore and gangue mineralogy, as well as their paragenetic and textural relationships within the different lithological units and drill-cores.

Detailed mineralogical characterization was conducted on both the milled drill-core samples and HLS sinks by SEM-based AM using a Mineral Liberation Analyzer (MLA; Gu, 2003). The MLA analyses were performed using a Thermo Fisher Scientific FEI Quanta 650F field emission gun SEM at the HIF, equipped with two Bruker Quantax X-Flash 5030 energy dispersive X-ray spectrometers. Measurement and data processing were accomplished using the MLA software suite (versions 3.1.4.686 and 3.1.5.993, respectively).

A grain-based X-ray mapping (GXMAP) routine, as well as a sparse phase liberation X-ray mapping routine (SPL-GXMAP) were used for analyses (Fandrich et al., 2007). The former represents a comprehensive particle mapping measurement, where both ore and gangue minerals are mapped until a particle count limit of 200,000 is reached. The latter represents a BSE thresholding mapping technique, where minerals exceeding a predefined BSE brightness are mapped. This technique improves the counting statistics of minor and trace minerals (e.g., sulfides) by removing particle count restrictions. This allows for quantitative mapping of bright minerals over the entire surface area of each epoxy mount. The total bright phase content was obtained from the GXMAP measurement, whereas the relative proportions of each bright phase were obtained from the SPL-GXMAP measurement. Further information on operating conditions used for the MLA is listed in Table A3 (ESM-1).

3.4. Mineral chemistry

Twelve grain mount samples (HLS sink; 25 mm) containing sufficient mineral sulfide content (> 0.1%), including three from the S1 (footwall sandstone), five from the T1 (Kupferschiefer), and four from the Ca1 (hanging wall Zechstein limestone) lithological units, were selected for sulfide mineral chemical analysis. Prior to EPMA and LA-ICP-MS measurements, all polished mounts were examined using reflected-light microscopy and SEM to identify suitable analytical points and to avoid

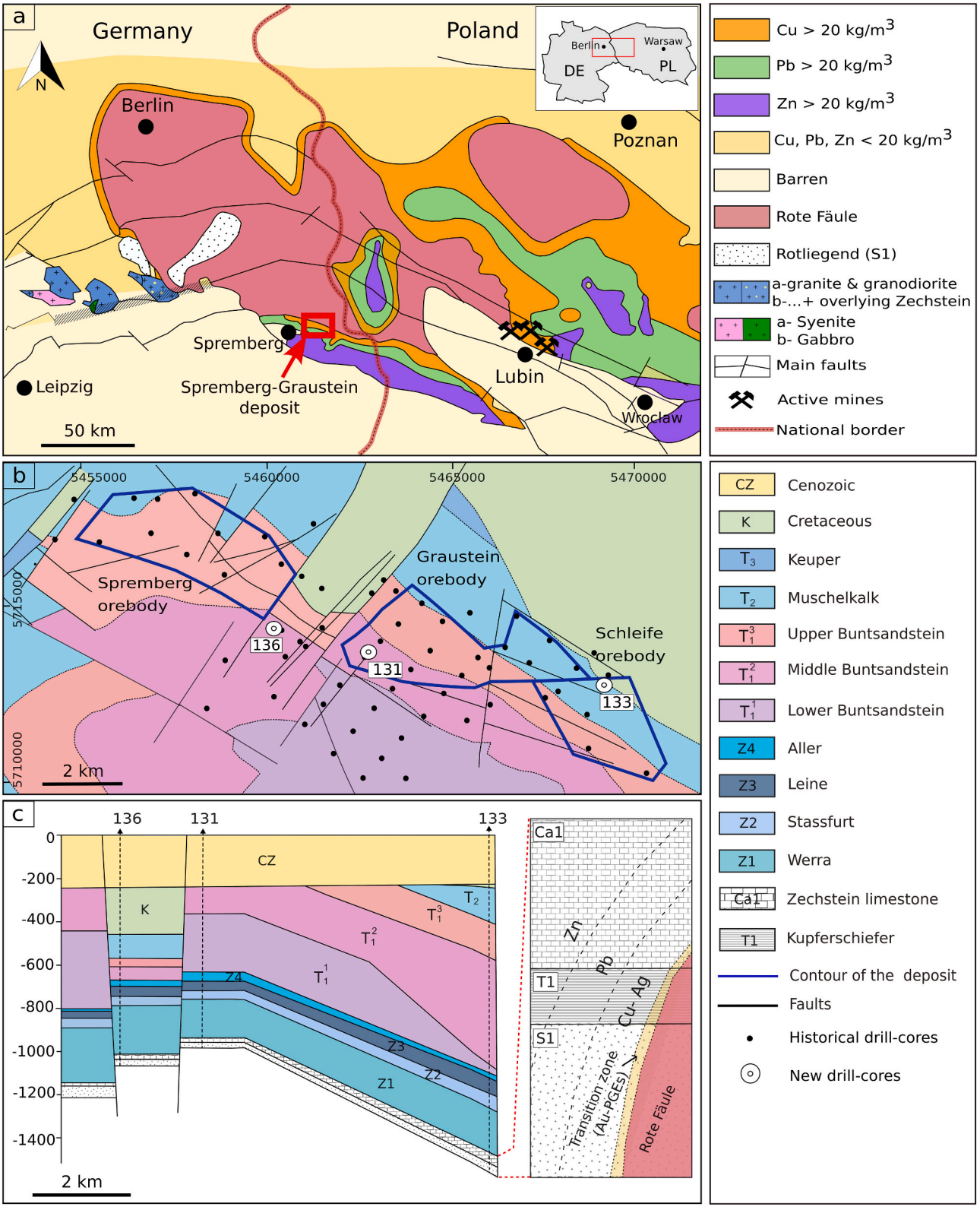

Fig. 1. a) Simplified geological map of South Brandenburg and Lower Silesia showing metal zonation in the T1 unit (modified after Kopp et al., 2010). The location of the Spremberg-Graustein-Schleife prospect is indicated in red. Inset: DE: Germany; PL: Poland. b) Geological map of the Spremberg-Graustein-Schleife prospect area. This map shows the geological units exposed below Cenozoic cover (modified after Kopp et al., 2006). Coordinates are in Gauss-Krüger projection. c) Cross section showing the stratigraphy and location of the three drill-cores and a simplified cross section illustrating the metal zonation in the main three lithological units S1 (Rotliegend sandstone), T1 (Kupferschiefer) and Ca1 (Zechstein limestone). (For interpretation of the references to colour in this figure legend, the reader is referred to the web version of this article.)

mineral inclusions and intergrowths that could affect the analytical results. LA-ICP-MS was employed to analyze the major sulfide minerals (Cu-, Pb-, Zn-, and Fe-sulfides) to quantify trace element concentrations, including the concentrations of the four target elements (Co, Ni, As, Bi). Sulfosalts and arsenides were analyzed primarily by EPMA and SEM-EDS, as the target elements in these minerals occur at major-element levels. Where possible, LA-ICP-MS was additionally applied (e.g., to quantify Co, Ni, and Bi in tennantite), though the number of analyses is limited due to their fine grain size and trace abundance. Only sulfides, sulfosalts, and arsenides were measured for mineral chemical analysis, since they represent the major mineral groups recovered during froth flotation in the processing plant.

EPMA analyses were conducted using a JEOL JXA-8530F at the HIF (see Nourizenouz et al., 2026 for analytical methodology). The trace element content of sulfide minerals was studied by LA-ICP-MS at the Laboratory of Environment and Raw Materials Analysis (LERA), Karlsruhe Institute of Technology, with a focus on constraining the concentrations of Co, Ni, Bi, and As. The LA-ICP-MS system at LERA couples a Teledyne 193 nm Excimer Laser to a Thermo Fisher Scientific Element XR sector-field ICP-MS. Samples were ablated in a helium atmosphere and mixed with argon and nitrogen before reaching the plasma torch. The ICP-MS was tuned for maximum sensitivity while keeping oxide formation (UO/U $< 0.1\%$) and element fractionation (i.e., Th/U ≈ 1) low. An ablation pulse frequency of 10 Hz and fluence of 5 J/cm^2 for 25 s were employed. A 50 μm spot size was preferentially used where grain size and texture permitted, while smaller spot sizes (down to 20 μm) were employed in areas affected by intergrowths or inclusions to minimize mixed analyses. For galena, a constant spot size of 20 μm was used due to its high signal intensity.

Where possible, a minimum of 5 spot analyses were performed on each mineral in each sample. The following isotopes were measured, each with 20 ms dwell time, except when in parenthesis: ^{23}Na, ^{27}Al, ^{29}Si, ^{32}S (8 ms), ^{33}S (8 ms), ^{39}K, ^{43}Ca, ^{44}Ca, ^{51}V, ^{55}Mn, ^{57}Fe (8 ms), ^{59}Co, ^{60}Ni, ^{63}Cu, ^{66}Zn, ^{69}Ga, ^{71}Ga, ^{72}Ge, ^{73}Ge, ^{74}Ge, ^{75}As, ^{78}Se (80 ms), ^{95}Mo (80 ms), ^{105}Pd (80 ms), ^{107}Ag, ^{111}Cd, ^{113}In (40 ms), ^{115}In (40 ms), ^{118}Sn, ^{121}Sb, ^{125}Te (80 ms), ^{126}Te (80 ms), ^{137}Ba, ^{185}Re (120 ms), ^{187}Re (120 ms), ^{189}Os (80 ms), ^{195}Pt (80 ms), ^{197}Au (80 ms), ^{202}Hg, ^{205}Tl, ^{208}Pb, and ^{209}Bi (80 ms). Two spots on each of four different reference materials were measured before and after every 40 spot analyses, allowing for the correction of instrumental drift over the course of an experiment. The reference materials included MASS-1 polymetallic sulfide (Wilson et al., 2002), MUL-ZnS1 sphalerite (Onuk et al., 2017), UQAC-FeS-4 base metal sulfide nano-powder pellet (Savard et al., 2018), and NIST SRM 612 glass (Jochum et al., 2011).

Data reduction was performed using the HDIP software package from Teledyne. Time-resolved LA-ICP-MS signal profiles were examined for each analysis to assess and mitigate the effects of fine-grained inclusions. Distinct signal spikes or peaks indicative of inclusions were identified and excluded during data reduction. To convert measured count rates into concentrations, the ^{63}Cu signal was used as the internal standard for Cu-sulfides (chalcocite and covellite), as well as bornite, while ^{57}Fe was used for chalcopyrite and pyrite. For sphalerite and galena, ^{66}Zn and ^{208}Pb were used as internal standards, respectively. Internal standard concentrations were derived from the average concentrations of the corresponding elements within each mineral generation in each sample, as determined from prior EPMA measurements. Different external standards were selected to match the matrix for the different sulfide minerals. MASS-1 was used for Cu(Fe) sulfides, UQAC-FeS-4 for pyrite, and MUL-ZnS1 for sphalerite and galena. NIST SRM 612 was measured for quality control and drift monitoring.

3.5. Elemental deportment and uncertainty Assessment

The elemental deportment of Co, Ni, As, and Bi was quantified by calculating the contribution of target minerals to the total metal content, following the methodology described by Frenzel et al. (2019). Bootstrap re-sampling was used to estimate the uncertainties on the modal mineralogy measurements, while Monte Carlo simulations were applied for uncertainties on the mineral chemical data for both sulfides and the discrete Co, Ni, and As minerals. The simulation results from SEM-based AM, EPMA, and LA-ICP-MS were integrated to determine the best estimates and 95% confidence intervals for each metal deportment in each sample. To ensure representative, accurate, and internally consistent results, each dataset was validated through multiple quality control measures. A detailed account of these quality assurance protocols is provided in Nourizenouz et al. (2026).

4. Results

In the following sections, the results of the bulk geochemical, mineralogical, and mineral chemical analyses are presented. Further details used for this assessment are provided in the electronic supplements (ESM-1, −2, and − 3).

4.1. Bulk geochemistry

A comparison of assay results from this study and existing company data shows good overall agreement, confirming the reliability of the sampling and sample preparation (Fig. A2). Minor Co contamination, likely from the grinding media, was identified in a number of sandstone samples. Accordingly, KSL data were utilized for this element (see ESM-1). Contamination was not identified for any of the other elements.

The results indicate that the T1 unit is enriched in base metals across all three drill-cores (Table 1, ESM-2). Notably, the T1 interval exhibits high Cu concentrations with average concentrations of 5.3 wt% and 1.2 wt% in drill-cores 131 and 133, respectively, and average Pb and Zn contents of 1.8 wt% and 0.5 wt%, respectively, in drill-core 136. The highest contents of Co and Ni are also found within the T1 unit. For example, the highest average Co content occurs in the T1 unit of drill-core 131 (178 μg/g) and the highest average Ni content occurs in the T1 unit of drill-core 136 (116 μg/g). Arsenic is also abundant in the T1 unit. However, drill-core 136 exhibits elevated As contents in both the underlying S1 unit (47 μg/g) and the overlying Ca1 unit (up to 120 μg/g in sample 136–1). Bismuth concentrations are much lower, ranging from 0.1 to 12.2 μg/g, and show a distinct positive correlation with Cu ($R^2 = 0.73$).

4.2. Mineralogy

4.2.1. Qualitative mineralogy

The mineral assemblages in the drill-cores reflect the expected stepwise interaction between metalliferous brines and early diagenetic pyrite (Borg et al., 2012 and references therein). This interaction resulted in a temporal and spatial sequence of: Fe-oxides (Fe^{3+}, Rote Fäule oxidation front) → Cu(Fe)-sulfides and electrum (Au–PGEs) → chalcocite group minerals (hereafter chalcocite) and bornite (Cu) → chalcopyrite/bornite (Cu) → galena (Pb) → sphalerite (Zn) → pre-ore pyrite (Fe^{2+}) (Fig. A1). Within this framework of base metal sulfide zonation, the occurrence and abundance of minerals containing Co, Ni, and As in stoichiometric amounts vary systematically between different zones. In the oxidized zone, sulfides, sulfosalts, and arsenides are absent. In the Au–PGE zone, sulfosalts and arsenides are not present, and sulfides remain scarce; however, selenide minerals, such as clausthalite and electrum grains, are hosted within ore-forming Cu-sulfides.

In the Cu-mineralized zone, minerals from the cobaltite (CoAsS) – gersdorffite (NiAsS) solid solution series (hereafter cobaltite – gersdorffite) commonly occur as very fine-grained inclusions within ore-forming Cu(Fe)-sulfides. In samples dominated by chalcopyrite/bornite, minute inclusions of cobaltite – gersdorffite are found alongside tennantite, which itself forms intergrowths with Cu(Fe)-sulfides (Fig. 2a). Such inclusions are particularly common in the T1 stratigraphic unit, where they occur as vermicular intergrowths within

Table 1
Whole rock geochemical assays for Cu, Co, Ni, As and Bi.

Drill-core	Composites	Lithology	Cu (%)[a]	Co (µg/g)	Ni (µg/g)	As (µg/g)	Bi (µg/g)
			0.2 µg/g	0.5	0.5	0.5	0.1
131	131–1	Ca1	0.070	29.9	12.0	38.5	0.4
	131–2	Ca1	1.50	7.4	14.5	14.6	0.1
	131–3	Ca1	2.21	7.8	21.5	9.8	0.2
	131–4	T1	5.28	178.3	169.0	78.9	12.2
	131–5	S1	1.96	6.0	16.3	9.1	3.3
	131–6	S1	1.08	2.1	17.1	1.4	0.5
	131–7	S1	1.01	3.1	16.9	1.0	0.4
	131–8	S1	0.21	3.7	19.4	3.0	0.1
133	133–1	Ca1	0.003	3.0	7.2	4.4	< 0.1
	133–2	Ca1	0.003	2.5	4.6	4.2	< 0.1
	133–3	Ca1	0.038	18.0	20.6	21.9	0.1
	133–4	T1	2.22	48.7	50.9	51.6	0.8
	133–5	T1	0.100	7.8	28.3	5.3	0.5
	133–6	S1	0.004	4.1	20.6	4.9	< 0.1
136	136–1	Ca1	0.839	68.3	29.5	120.0	0.5
	136–2	Ca1	0.035	14.5	24.0	53.3	0.1
	136–3	T1	0.15	8.2	69.7	17.0	0.2
	136–4	T1	0.171	54.0	76.0	33.2	0.2
	136–5	S1	0.103	40.8	47.5	46.5	0.1

[a] For Cu, two different methods were used: ICP-MS was conducted on all samples. ICP-OES was conducted on samples with Cu content exceeding the upper limit of detection of the ICP-MS (1 wt%). Please note that the lower detection limits are provided directly below the element.

chalcocite and bornite (Fig. 2b). Fine inclusions of cobaltite – gersdorffite are also widespread in proximity to the S1-T1 contact, where they occur as infills or replacements of fine-grained framboidal pyrite (Fig. 2c, d). Disseminated grains of the safflorite ($(Co,Fe)As_2$) – rammelsbergite ($NiAs_2$) solid solution series (hereafter safflorite – rammelsbergite) were found in the T1 unit of drill-core 133. These minerals occur in massive and otherwise featureless calcite as rare pore infills or isolated grains. Using location coordinates from SEM-based AM, it was found that these grains are concentrated within a well-defined band (Fig. 2e; A3). SEM-EDS elemental mapping was used to confirm the presence and distribution of Co, Ni, and As (Fig. 3). The cobaltite – gersdorffite grains exhibit elevated levels of both Co and Ni (Fig. 3a, b, c). The same holds true for safflorite – rammelsbergite, which also commonly contains highly variable contents of both Co and Ni within individual grains (Fig. 3d). In the Pb-Zn-mineralized zone, only a small number of cobaltite – gersdorffite grains were identified and were typically associated with pyrite.

Several additional trace minerals, which contain Co, Ni, and As, were identified by SEM-based AM. These include minute, isolated grains of millerite (NiS) in the Cu-mineralized zones, as well as minerals of the linnaeite ($Co^{2+}Co^{3+}{}_2S_4$) – polydymite ($Ni^{2+}Ni^{3+}{}_2S_4$) solid solution series (hereafter linnaeite – polydymite). The latter occur in the sandstone intervals of drill-core 136 and are typically associated with chalcopyrite and pyrite. Minerals containing Bi in stoichiometric proportions were not identified by SEM-based AM in any of the samples.

4.2.2. Quantitative mineralogy

Quantitative mineralogical data were obtained using SEM-based AM and were complemented by results from X-ray powder diffractometry (see Nourizenouz et al., 2026 for the complete dataset). The normalized modal mineralogy results for the major sulfides, obtained from GXMAP and SPL-GXMAP measurements, show good agreement, indicating that the collection of 200,000 grains per sample in the GXMAP mode was sufficient to be representative of the entire grain mount (Fig. A4). In addition, the relative sulfide abundances in both drill-core samples and HLS sinks were compared to ensure the representativeness of the HLS technique further information is available in Nourizenouz et al. (2026).

The mineralogy of major gangue minerals varies greatly between the S1, T1, and Ca1 units (Fig. 4). The S1 unit (footwall sandstone) is dominated by quartz, along with clay minerals, K-feldspar, and carbonate group minerals. The T1 (Kupferschiefer) and Ca1 (hanging wall carbonates) units, in contrast, are carbonate-rich (dolomite and calcite), and are accompanied by moderate to minor concentrations of illite, muscovite, and quartz. The T1 unit further shows variable enrichment in organic carbon (0.3–9.7 wt%).

Sulfide mineralogy also varies across lithologies and drill-cores. In drill-core 131, samples from all three units (S1, T1, and Ca1) belong to the Cu-mineralized zone, with chalcocite and bornite representing the dominant Cu-sulfide minerals. In the lower part of drill-core 133 (S1 and the base of the T1 unit), a general absence of sulfides coincides with the Rote Fäule oxidation front. Like drill-core 131, samples from the T1 unit belong to the Cu-mineralized zone. However, the overlying Ca1 unit is Pb-mineralized and contains abundant galena and pyrite. Most samples from drill-core 136 belong to the Pb-Zn-mineralized zone (galena and sphalerite). In contrast, the uppermost Ca1 unit contains Cu mineralization, such as bornite, chalcopyrite, and covellite. Although Co, Ni, and As minerals are scarce (<0.03 wt%) in all three drill-cores, they are generally more abundant in Cu-rich samples (Fig. 4).

4.3. Mineral chemistry

At stoichiometric levels, Co, Ni, and As occur in a variety of minerals, including arsenides (e.g., safflorite – rammelsbergite) and sulfosalts (e.g., cobaltite – gersdorffite, tennantite, etc.). They are also present in minor to trace concentrations in several major sulfide minerals, such as pyrite, marcasite, chalcopyrite, chalcocite, bornite, sphalerite, and galena. Hereafter, we refer to the former group of minerals as Co, Ni, and As minerals and the latter as major sulfide minerals. Since discrete Bi minerals were not identified during the comprehensive SEM-based AM searches, its occurrence is limited to minor contents substituted into the lattice of major sulfide minerals. The following sections describe the results obtained for the mineral chemistry of different Co, Ni, and As minerals, as well as the major sulfide minerals (refer to ESM-3 for detailed results).

4.3.1. Cobalt, nickel, and arsenic minerals

Cobaltite – gersdorffite contains both Co and Ni in all analyzed grains, with Ni ranging from 8 to 17 wt% and Co from 21 to 29 wt%; however, the sum of Co and Ni across the analyzed points remains roughly constant, averaging 36 wt%, as expected for this mineral series. The As and S contents are also constant, averaging 39 wt% and 23 wt%, respectively (Fig. 5a). Although the molar As/S ratio is thus somewhat low for stoichiometric cobaltite – gersdorffite series minerals, minor deviations may be attributed to substitution of As by S, or alternatively,

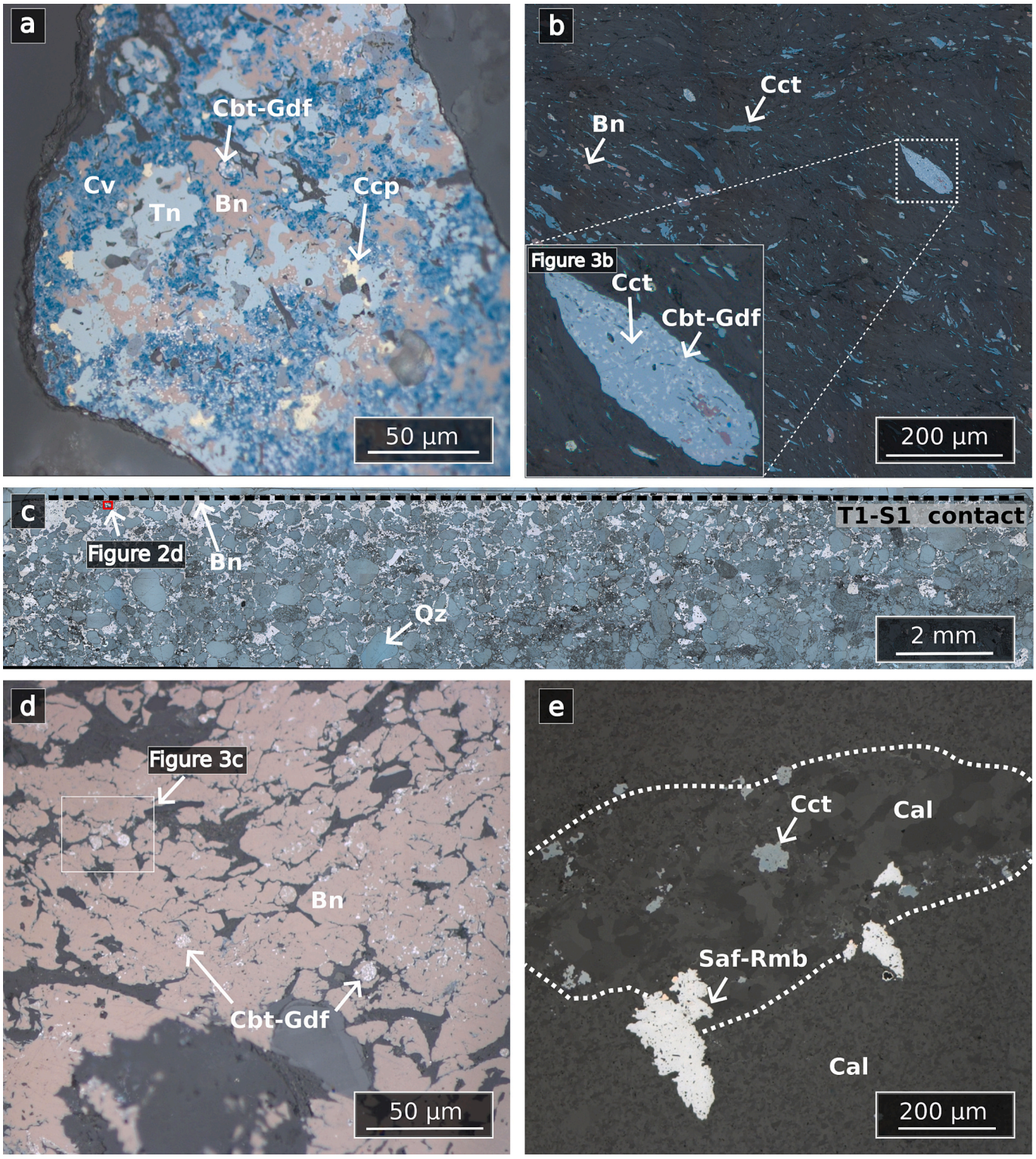

Fig. 2. Reflected light photomicrographs of Co, Ni, and As minerals from the Spremberg-Graustein-Schleife prospect. a) A complex sulfide particle from the Ca1 unit, showing fine inclusions of cobaltite – gersdorffite (Cbt-Gdf) within a composite particle composed of tennantite (Tn), chalcopyrite (Ccp), bornite (Bn) and covellite (Cv) from sample 136–1. b) Sample 131–4 (T1 unit) with disseminated bornite and chalcocite (Cct) with fine vermicular inclusions of cobaltite – gersdorffite within chalcocite. c) Contact between the S1 and T1 units in sample 131–5. Note the abundance of bornite along this contact. d) Bornite along the S1-T1 contact with abundant inclusions of cobaltite – gersdorffite. e) Sample 133–4 (T1 unit) showing disseminated safflorite – rammelsbergite (Saf-Rmb), along with chalcocite in a calcite-dominated (Cal) matrix.

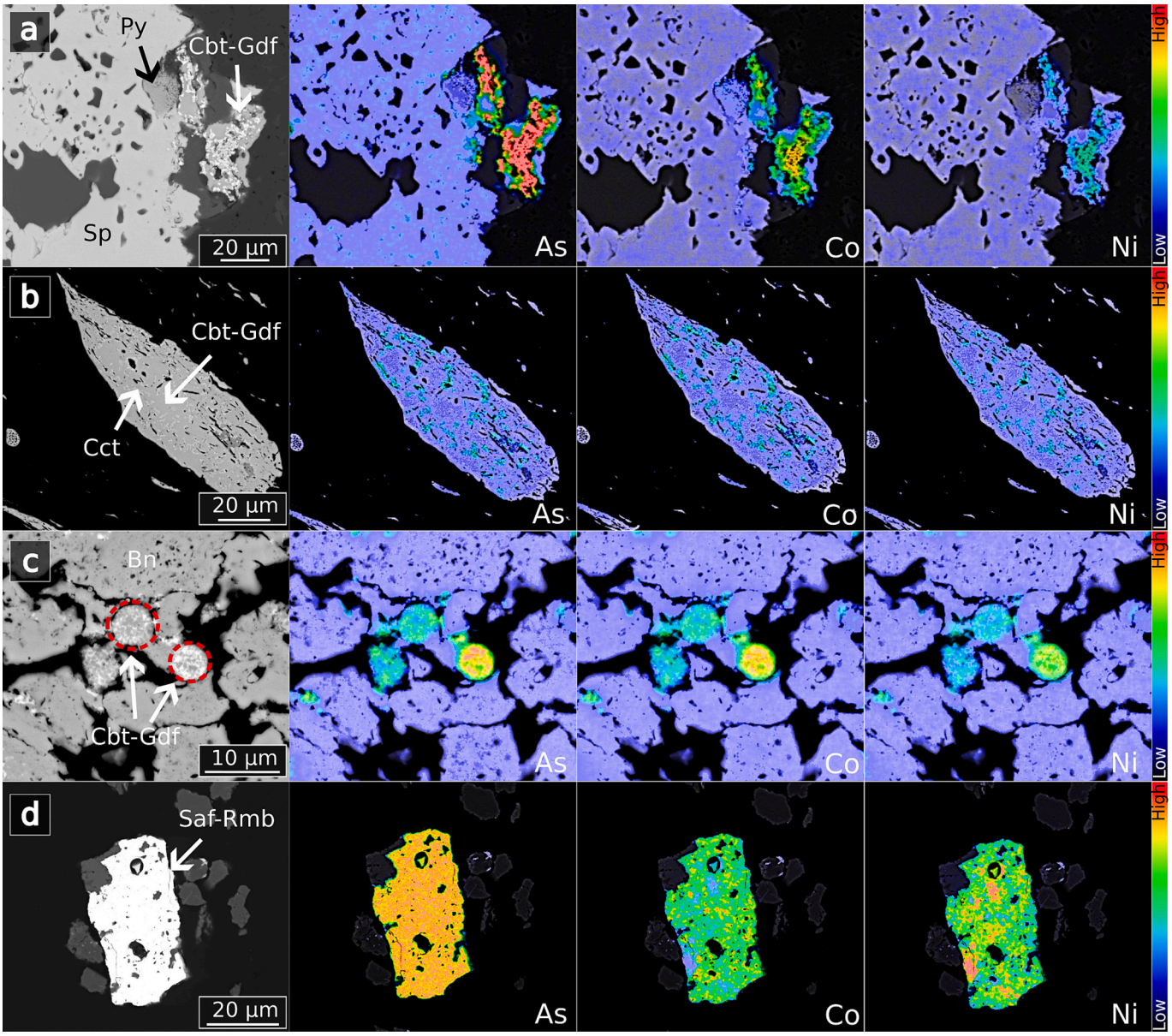

Fig. 3. SEM-BSE images and elemental maps of Co, Ni, and As minerals. a) Cobaltite – gersdorffite associated with sphalerite (Sp) in a sample from the Ca1 unit (HLS sink from sample 131–2). b) Cobaltite – gersdorffite inclusions within chalcocite from the T1 unit (sample 131–4). c) Cobaltite – gersdorffite infilling framboidal pyrite in the S1 unit near the contact with the T1 unit (sample 131–5). d) Safflorite – rammelsbergite-bearing particle with variable Co and Ni contents in the HLS sink from the T1 unit (sample 133–4).

to deviations caused by the influence of surrounding sulfide minerals enclosing the minute (<3 µm) grains of cobaltite – gersdorffite. In fact, the latter is suggested by the often elevated Cu and/or Zn values in the chemical data for these minerals (ESM-3, Fig. 5a).

Safflorite – rammelsbergite is characterized by rather consistent As values at ~71 wt% (Fig. 5b). Cobalt (13–21 wt%) and Ni (9–16 wt%) contents are variable (ESM-3), but again constant in their sum (~29 wt %). The S1 samples from drill-core 136 contain linnaeite – polydymite grains with compositions of 42 wt% S, 32 wt% Co, 23 wt% Ni, and minor Fe (<3 wt%) (ESM-3). Cobalt and Ni contents were generally found to be constant across the different grains analyzed in this sample (Fig. 5c). Tennantite was observed in the Ca1 unit of drill-cores 131 and 136 (Fig. 5d). Its appearance corresponds with elevated bulk rock As concentrations (120 µg/g in sample 136–1).

4.3.2. *Major sulfide minerals*

An overview of the concentrations of the target elements (Co, Ni, As, and Bi) in major sulfide minerals obtained from LA-ICP-MS measurements is presented in Fig. 6, with further details provided in ESM-3. Among the major sulfide minerals, pyrite contains the highest concentrations of Co, Ni, and As, with average values of 155, 244, and 576 µg/g, respectively, across all samples. Pyrite in the T1 sample of drill-core 136 also displays particularly high Ni concentrations, reaching up to 1.5 wt%, with these spots additionally enriched up to 6 wt% in Cu (ESM-3). Chalcopyrite and covellite also contain elevated concentrations of these three elements. Chalcopyrite, in particular, can exhibit very high As concentrations in the S1 and T1 samples from drill-core 136, averaging 280 and 557 µg/g, respectively (Fig. 6). All Cu(Fe)-sulfides, including chalcocite and bornite, in the S1 samples are relatively depleted in Co, Ni, and As compared to those in the T1 and Ca1 units, with most analytical spots falling below detection limits (BDL). Elevated contents of Co, Ni, and As are occasionally found within all sulfides. However, in cases where the concentrations of these elements covary, they are related to the presence of minute/sub-microscopic inclusions of

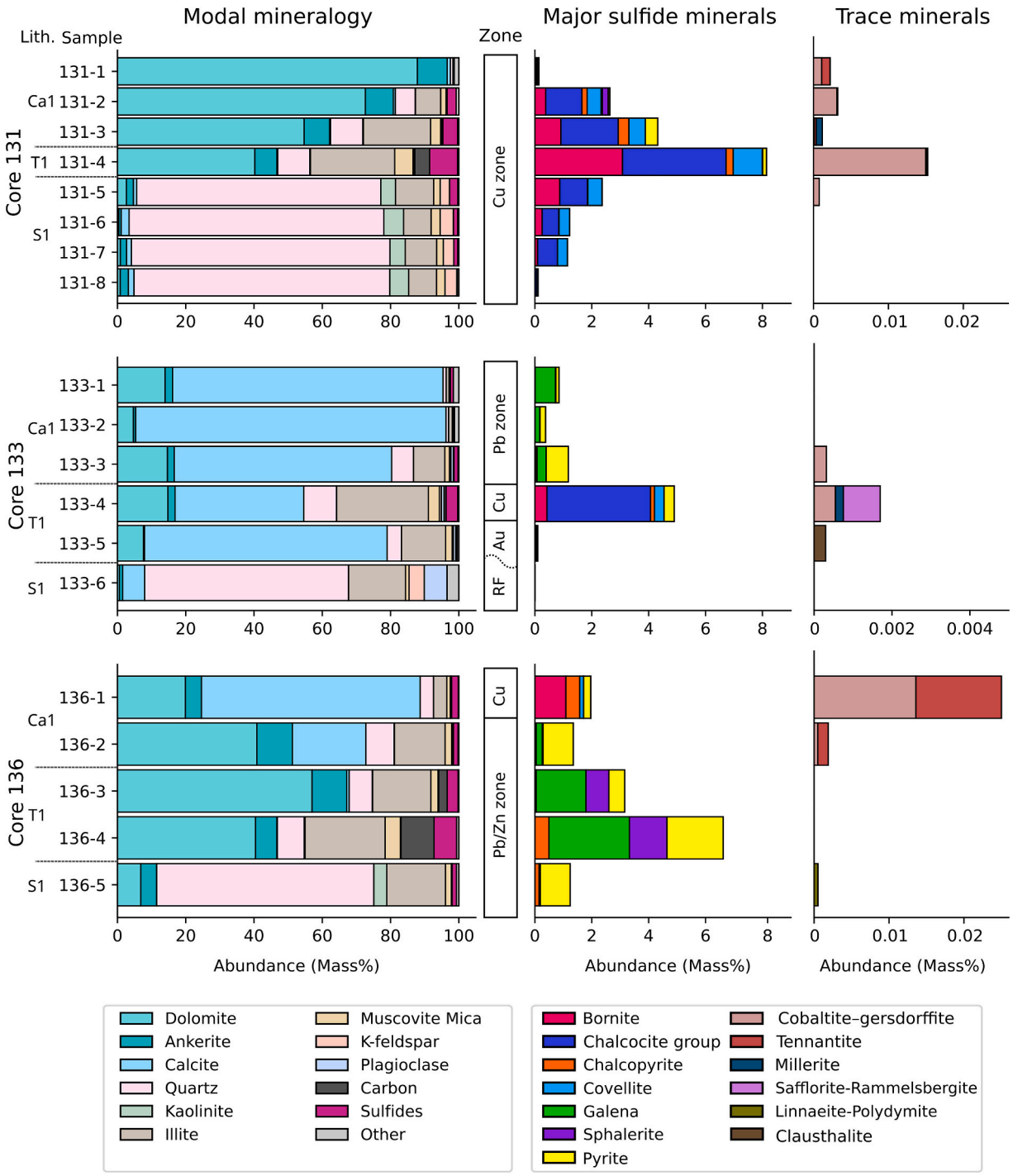

Fig. 4. Modal mineralogy, major sulfide (after Nourizenouz et al., 2026) and trace mineral abundances of the composite samples from SEM-based AM. Note variable x-axis ranges for the trace minerals.

cobaltite – gersdorffite.

Bornite, particularly in samples from the S1 and T1 units, is enriched in Bi, with average concentrations of 142 μg/g and 209 μg/g, respectively. In drill-core 133, bornite and chalcocite in the sample corresponding to the lower part of the T1 unit contain significantly more Bi than the sample representing the upper part of this unit. At the lower T1 interval in this drill-core, the Rote Fäule intersects the T1 unit. Minute inclusions of clausthalite (PbSe) are limited to Cu-sulfides from this particular sample. Galena also hosts Bi; although its Bi content is lower than bornite, it remains remarkably constant across all three drill-cores and lithologies (~ 9 μg/g).

Time-resolved LA-ICP-MS spot profiles for individual spot analyses are presented in Fig. 7. These plots provide insights into the mode of trace element incorporation within mineral structures (Cook et al., 2011; Gregory et al., 2015). Flat signal patterns in the time-resolved LA-ICP-MS data typically indicate that trace elements are either structurally incorporated into the host mineral lattice or that they occur as uniformly distributed nano-scale inclusions. Such patterns were observed for Bi in bornite, As in chalcopyrite, and Co, Ni, and As in pyrite. In contrast, localized spikes in the profiles for chalcocite group minerals and bornite indicate the presence of Co, Ni, and As as minute mineral inclusions. This is consistent with petrographic observations, where abundant fine

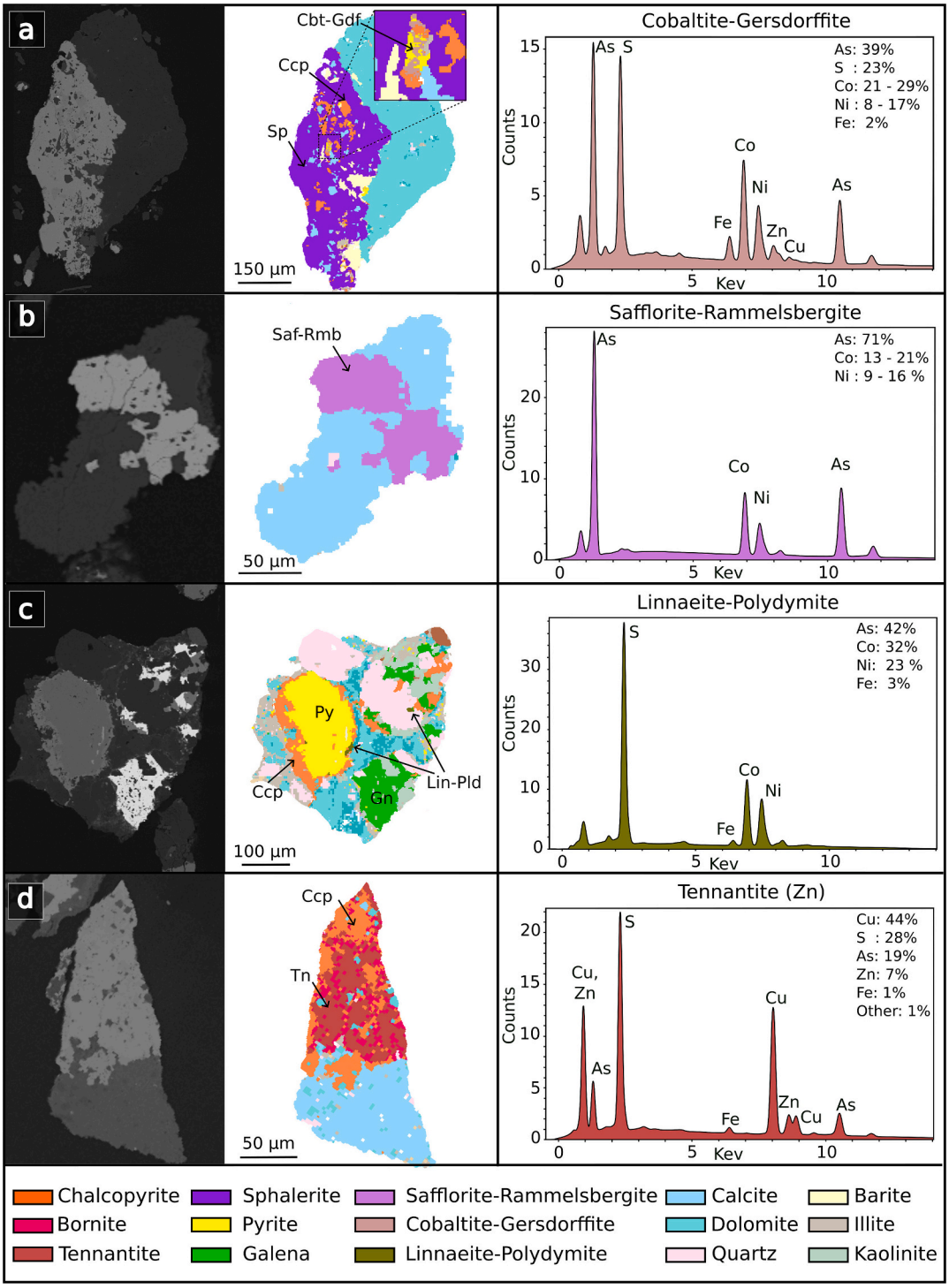

Fig. 5. SEM-BSE images, MLA mineral maps, and SEM-EDS spectra of selected particles containing: a) cobaltite – gersdorffite (note the occurrence of peaks characteristic of Cu and Zn in the X-ray spectrum, which is attributed to the surrounding chalcopyrite and sphalerite); b) safflorite – rammelsbergite (note the variable Co and Ni contents); c) linnaeite – polydymite (Lin-Pld); d) tennantite. The mineral chemical compositions for a) and c) are derived from average SEM-EDS values, whereas those for b) and d) are derived from EMPA.

inclusions of cobaltite – gersdorffite were observed within major sulfide mineral grains, specifically bornite and chalcocite.

4.4. Element deportment

The element deportment in each sample was quantified by integrating modal mineralogical compositions from SEM-based AM with mineral chemical data from LA-ICP-MS and EPMA (Fig. 8, ESM-1). The results reveal that Co, Ni, and As show close similarities in their deportment. Sulfosalts and arsenides, which are generally only present in trace amounts in the bulk ore, are the most important hosts for these three target elements. In the Cu-mineralized samples, cobaltite – gersdorffite is a major host of these three elements. Although millerite and tennantite occur only in very minute amounts, they constitute important hosts for Ni and As, respectively, wherever they are present (e.g., millerite in sample 131–3 and tennantite in sample 136–1). Pyrite and

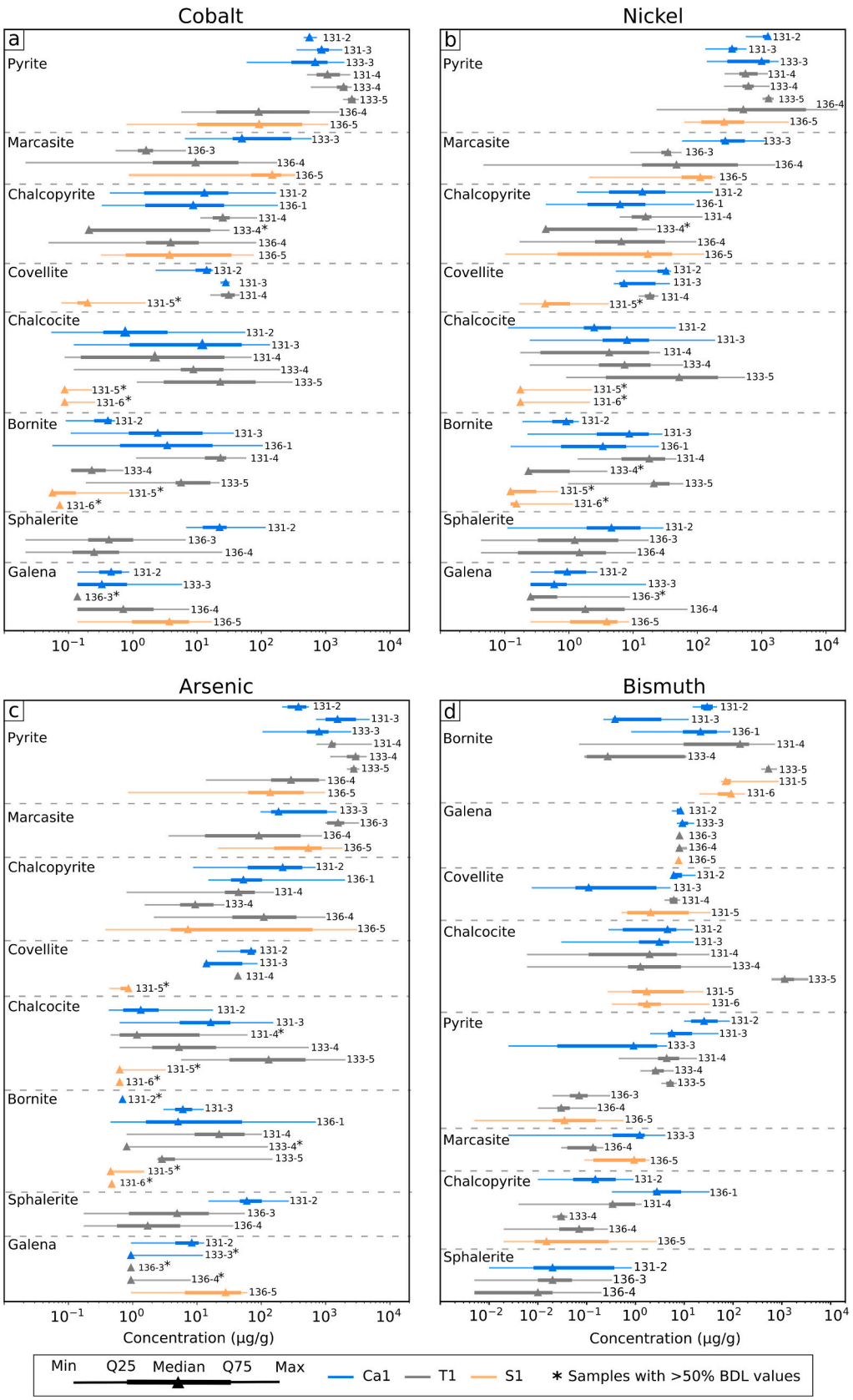

Fig. 6. Summary plots illustrating the main statistics of Co, Ni, As, and Bi concentrations in major sulfides and lithologies. Note change in mineral order for Bi.

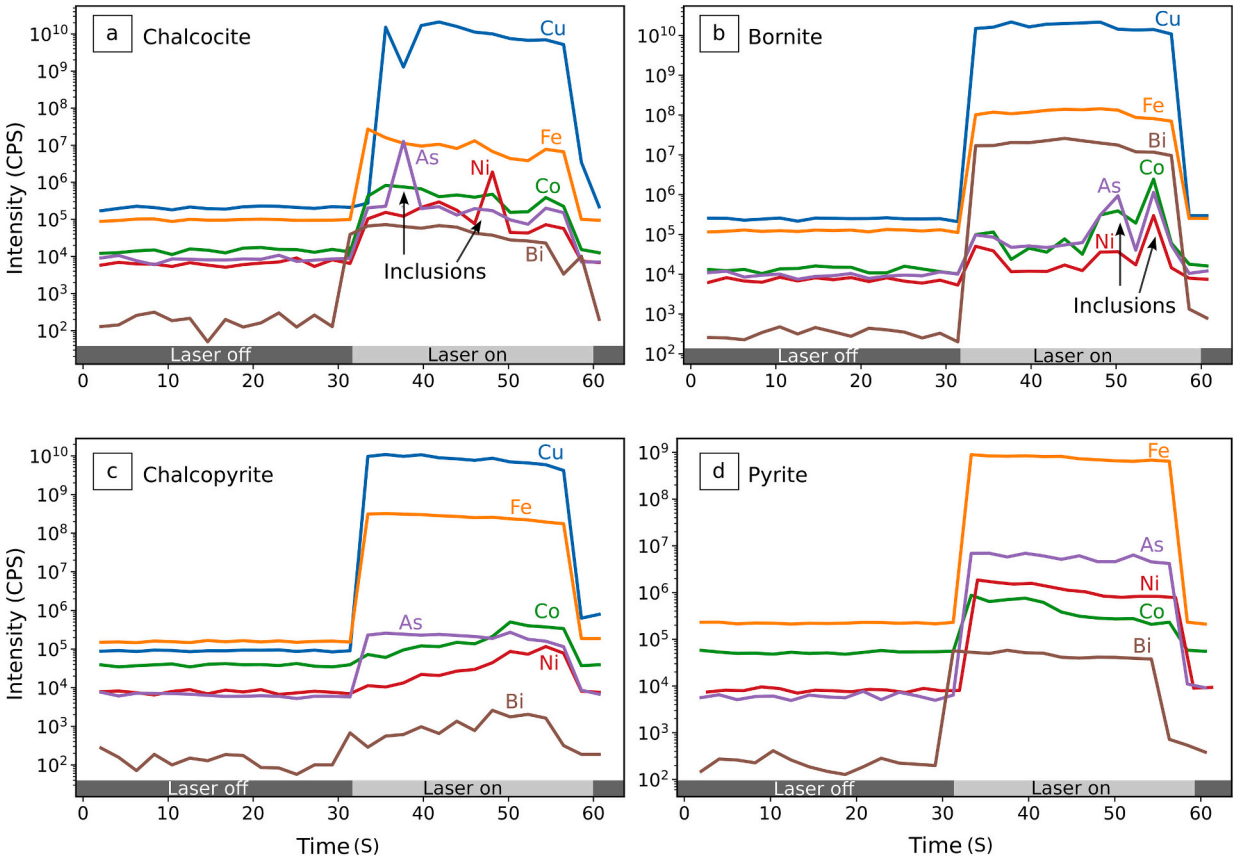

Fig. 7. Time-resolved LA-ICP-MS graphs showing individual analysis spots of a) chalcocite with As-, and Ni- bearing inclusions; b) bornite with As-, Ni-, and Co-bearing inclusions; c) chalcopyrite with elevated As content; d) pyrite enriched in As, Ni and Co. Time-resolved intensities expressed as counts-per-second (CPS) on a logarithmic scale.

chalcopyrite are major hosts of Co, Ni, and As in Pb-Zn-mineralized samples.

As expected from the SEM-based AM observations, Bi is hosted mostly by the major sulfides. In the Cu-mineralized zone, Bi is hosted primarily by Cu(Fe)-sulfides (mainly bornite and chalcocite), whereas in the Pb-Zn-mineralized zone, Bi is mainly hosted by galena and pyrite. Note that the deportment results for sample 131–6 (a sample from the S1 unit) are not shown due to very low bulk concentrations of all four target elements.

4.5. Validation of analytical results

Reconciliation between measured and calculated bulk concentrations from SEM-based AM and mineral chemistry data was carried out to assess whether all target elements are hosted within the recoverable minerals analyzed (Fig. 9). Among the four elements measured, the median calculated values of Bi are most congruent with measured concentrations. Similarly, good agreement between the measured and calculated values was noted for As, with the exception of two low-grade samples from the T1 unit. For Co and Ni, underestimation is more pronounced, particularly for Ni in the T1 unit. Note that some of the calculated assay values for Co, Ni, and As show high uncertainties.

5. Discussion

In this study, we examined the distribution of Co, Ni, As, and Bi within sulfosalts, arsenides, and major sulfide minerals to quantify the amounts of recoverable Co and Ni as potential by-products, and As and Bi as deleterious elements. Our results indicate that the calculated bulk contents of Co and Ni are underestimated relative to the assay values. For As, underestimation is less pronounced and only occurs in a small number of samples, with calculated values generally in good agreement with the measured assay values, considering the 95% confidence intervals. For Bi, the calculated values are closely aligned with the assays. In the following subsections, we first discuss potential reasons for the underestimation of Co, Ni, and As in some of the samples. We then examine the geological controls on elemental distribution and mineralization, followed by a discussion of the implications of these results for mineral processing.

5.1. Underestimation of calculated assays

The underestimation of Co, Ni, and As can be attributed to a number of factors relating to the intrinsic compositional and textural characteristics of Co, Ni, and As minerals in the Kupferschiefer-type orebody at the Spremberg-Graustein-Schleife prospect. For As, most samples fall along the 1:1 line considering the 95% confidence intervals (Fig. 9c). However, a small systematic underestimation is observed for samples characterized by very low bulk As concentrations (10 μg/g or less, Fig. 9c).

Cobalt and Ni show a stronger degree of systematic underestimation compared to As (Fig. 9). This can be attributed to the well-known substitution of these two transition metals into the crystal lattices of carbonates, silicates, Fe-oxides/oxyhydroxides, and other minerals (Slack et al., 2017). This is due to the similarity in charge and the ionic radii of Ni^{2+} (0.69 Å) and Co^{2+} (0.745 Å) to those of Fe^{2+} (0.78 Å), Fe^{3+} (0.645 Å), Mg^{2+} (0.72 Å), and Mn^{2+} (0.83 Å). Dolomite, as a major carbonate mineral in the samples from the Spremberg-Graustein-Schleife prospect, is enriched in Fe and Mn (Kim et al., 2024), and thus may also contain non-negligible concentrations of Co and Ni. Previous studies on

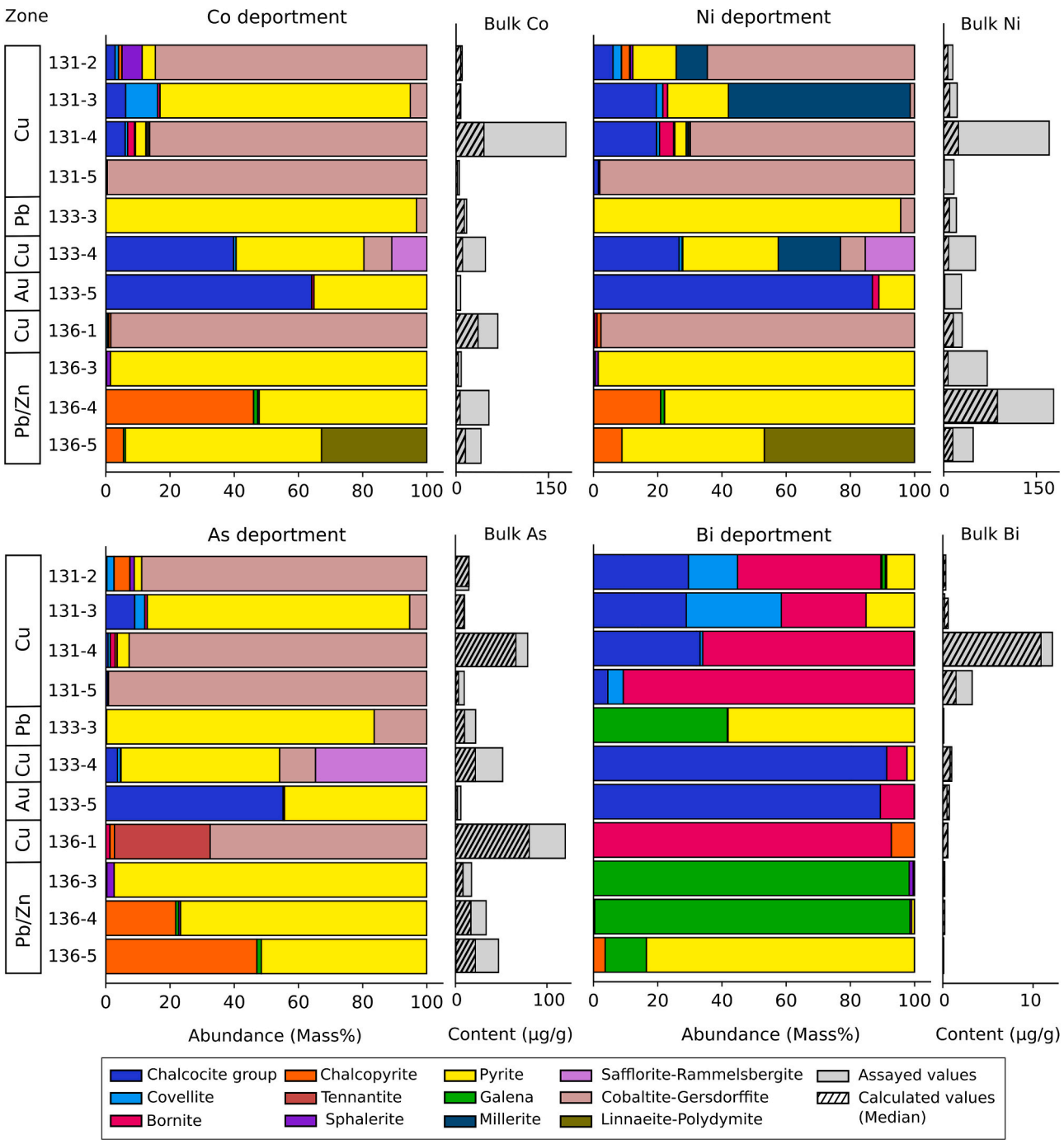

Fig. 8. Cobalt, nickel, arsenic, and bismuth deportment results.

Kupferschiefer samples from Poland have also suggested sheet silicates and feldspars as potential carriers of Co and Ni (Kucha and Pawlikowski, 1986; Mikulski, 2022). This is supported by LA-ICP-MS time-resolved elemental profiles of inclusion-rich sulfides in Kupferschiefer samples, where elevated (and highly variable) Co and Ni concentrations were documented from shale-hosted vein-type mineralization (Foltyn et al., 2022). Iron oxides and oxyhydroxides, such as hematite, magnetite, and goethite in the Rotliegend sandstones, as well as in samples cross-cut by the Rote Fäule oxidation front, may also serve as minor hosts for Ni and Co (Moats and Davenport, 2014). Finally, organic matter can also host Ni, as Sawłowicz (1985) reported the presence of Ni porphyrins in the resin fraction of bitumen from organic-rich, Cu-bearing shales of the Lubin-Sieroszowice mining district in Poland. We therefore attribute the systematic underestimation of Co and Ni in the calculated assays to the presence of these two metals substituted into different groups of gangue minerals.

The inherent textural characteristics of Co, Ni, and As minerals can also contribute to underestimation of calculated assays. Arsenides and sulfosalts represent the most important hosts of Co, Ni, and As, with respect to bulk rock content. However, these minerals are generally fine-grained and occur in trace abundances. The low overall abundance of these minerals and specifically their limited grain counts, may result in underrepresentation, contributing to discrepancies between calculated and assayed values. Further, they are not always homogeneously distributed, and in some instances occur as local clusters (e.g., safflorite – rammelsbergite), thus complicating accurate quantification of their

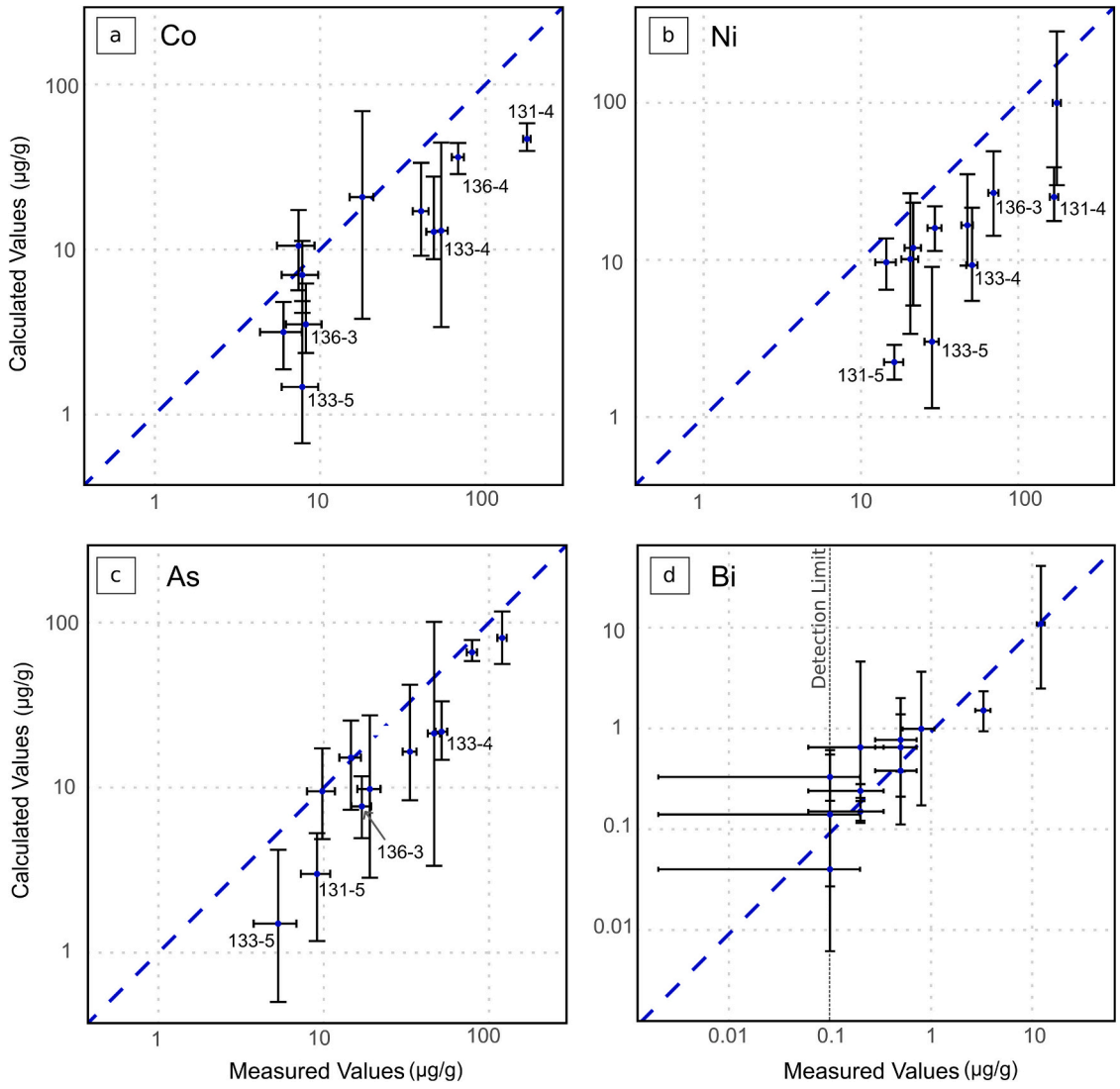

Fig. 9. Calculated whole rock concentrations versus measured (assayed) values in logarithmic scale, with estimated 95% confidence intervals for a) Co, b) Ni, c) As, d) Bi. Note the different scale for Bi compared to the other elements.

true abundance (nugget effect).

Based on the above, we conclude that consistent underestimation is mainly due to the presence of Co and Ni in gangue minerals. Yet, the limitations of SEM-based AM may also well contribute to systematic underestimation. One such limitation involves the segmentation of extremely fine-grained inclusions of Co, Ni, and As minerals (< 3 µm). When these fine-grained trace minerals occur as inclusions within sulfides, with similar mean atomic numbers (Z), their comparable grayscale intensities may hinder or even preclude grain segmentation. For example, Co, Ni, and As mineral inclusions (Z = 27.6–28.0) within bornite (Z = 25.4) and chalcocite (Z = 26.2) show weak BSE contrast and poor segmentation, whereas those in chalcopyrite (Z = 23.5) exhibit a stronger BSE contrast and improved segmentation. Similar challenges were observed for linnaeite – polydymite inclusions (Z = 22.4–22.9) within chalcopyrite. Moreover, when the target minerals occur in the form of inclusions within other sulfide minerals, the acquired X-ray spectrum (commonly a single analysis point) may represent a mixed analysis and be subject to misclassification, as the signal originates from the entire excitation volume rather than only the surface. Lastly, target mineral grain sizes below the minimum segmentation size of the MLA (~1 µm) may contribute to systematic underestimation. This is particularly well illustrated in Fig. 10, where samples that are characterized by extremely fine-grained Co, Ni, and As minerals (e.g., 131–4 and 133–4) are marked by significantly greater levels of underestimation compared to samples containing relatively coarse-grained Co, Ni, and As minerals.

5.2. *Uncertainties in calculated assays*

High uncertainties in calculated Co, Ni, and As assays mainly result from the compositional variability of different minerals. Both discrete Co, Ni, and As minerals, as well as the common major sulfides, especially pyrite, show considerable variation in Co, Ni, and As contents. Greater intra-grain and intra-sample variability increases the estimated standard deviations, which directly translates into greater uncertainty in the calculated bulk concentrations. Among the discrete Co, Ni, and As minerals, safflorite – rammelsbergite exhibits extensive intra-grain variability, with Co and Ni contents fluctuating significantly (Fig. 3d), while the As content remains relatively constant. Similar compositional heterogeneity has been reported by Wagner and Lorenz (2002) for diarsenide and sulpharsenide minerals from the Post-Variscan Co-Ni-Bi vein-type ores of the Bieber deposit (Spessart Mountains, Germany), which are also related to the Permian Kupferschiefer.

Compositional heterogeneity of pyrite and chalcopyrite is considered another reason for high uncertainties in Co, Ni, and As deportment calculations. Pyrite shows distinct compositional variability both within

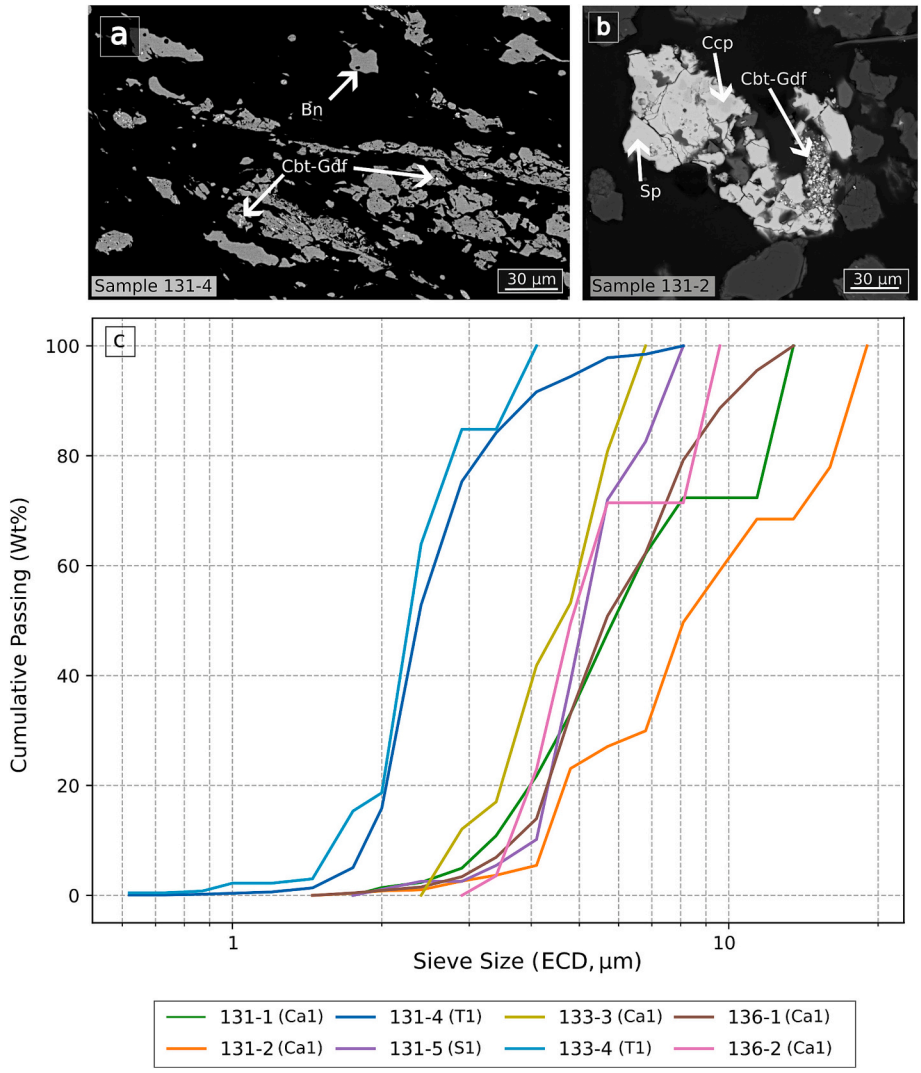

Fig. 10. Comparison of cobaltite – gersdorffite size distribution within different samples. a) Fine-grained cobaltite – gersdorffite in sample 131–4 (T1 unit). b) Coarse-grained cobaltite – gersdorffite in sample 131–2 (Ca1 unit). c) Cumulative mineral grain size distribution (GSD) plot.

different paragenetic generations and between different samples. In sample 136–4, for example, early framboidal pyrite, coarse euhedral pyrite, and vein-associated pyrite and marcasite are present. Marcasite and coarse euhedral pyrite are characterized by low Co, Ni, and As concentrations, while vein pyrite exhibits zones markedly enriched in Cu (up to 6 wt%) and Ni (up to 1.5 wt%). Since MLA cannot distinguish pyrite from marcasite, their combined abundances and contrasting compositions contribute to elevated uncertainties. In the same sample, chalcopyrite also shows strong variability in Co, Ni, and As, likely reflecting the different enrichment processes between vein-type and disseminated mineralization, as previously reported by Foltyn et al. (2022).

5.3. Spatial and temporal element distribution

The distribution of Co, Ni, and As in the studied samples marks distinct enrichment at the top of the S1 and at the base of the T1 units, corresponding to the transition from continental sandstones to reduced, organic-rich black marl/shale. This corresponds with previous studies (e.g., Kucha, 1990; Banas et al., 1996; Mikulski, 2022) and confirms that the geological redox interface acted as a key metal trap not only for major (Hitzman et al., 2005) but also for minor and trace elements. Cobaltite – gersdorffite grains are common along the S1-T1 interface and predominantly occur as infills of framboidal pyrite, a texture also observed in the Lubin-Sieroszowice district (Poland). Large et al. (1999) interpreted that framboidal pyrite acted as a preferred substrate for cobaltite precipitation, driven by local redox shifts along the S1-T1 contact.

Our results also reveal systematic differences in the deportment of trace elements across different zones of mineralization: In the Au-bearing basal T1 unit in drill-core 133, Cu-sulfides are not only notably enriched in Co, Ni, As, and Bi, but also contain clausthalite and rare electrum inclusions (Nourizenouz et al., 2026). This translates into a metal association rich in Ag, Se, Pb, Au, and Bi that has already been noted by Kopp et al. (2012). The latter authors related this association to a late-stage hydrothermal overprint of an earlier diagenetic Cu-Fe sulfide assemblage.

Beyond the immediate contact zone to the Rote Fäule, Cu-Ag-rich ores contain Co, Ni, and As, predominantly as minute discrete minerals – mostly as cobaltite – gersdorffite enclosed in the ore forming sulfide minerals. In the adjacent Pb-Zn-bearing mineralization zone, in contrast, the same elements substitute into the lattice of pyrite albeit at much lower bulk concentrations. Bi, however, does not form discrete mineral grains, and is substituted in Cu-sulfides and galena.

5.4. Implications for mineral processing

Although the Spremberg-Graustein-Schleife prospect has not progressed beyond the exploration stage, the deportment results reported in this study have important implications for the recovery of trace metals during beneficiation. Indeed, the significance of our results may be extended to active mining operations in Poland, where the process flowsheet involves the recovery of Cu-sulfides (and associated Ag) through froth flotation and the subsequent smelting of the flotation concentrate to yield refined Cu and Ag, along with Au, Pb, Re, and Ni as by-products (KGHMa). In this context, the deportment of Co and Ni is particularly relevant.

Exploration and exploitation of Kupferschiefer-type deposits in Central Europe primarily targets the Cu-Ag-mineralized zone. In this zone, Co and Ni, which are hosted by discrete arsenides and sulfosalts, are amenable to Cu-sulfide flotation. Cobaltite – gersdorffite occurs as fine inclusions within Cu-sulfides; given their close textural association with Cu-sulfides, they are expected to report to the Cu concentrate during flotation. Safflorite – rammelsbergite, in contrast, occurs mostly as discrete mineral grains that are not necessarily intergrown with Cu-sulfides. Nevertheless, they will still be recovered during flotation because the reagents used as collectors in Cu-flotation circuits promote the flotation of arsenides and sulfosalts (Stodulski and Drzymala, 2016; Dehaine et al., 2021).

A significant proportion of Co and Ni are hosted within gangue minerals particularly in the T1 unit. During flotation, these gangue minerals (with their contained Ni and Co) will be lost to the tailings stream, resulting in significant losses of these two valuable by-product metals. This loss appears unavoidable, unless mining operations return to the previous approach of simply smelting the entire T1 unit.

Arsenic and Bi represent two deleterious elements in Cu concentrates that were considered in this study. In the Cu-mineralized zone, As occurs mainly in cobaltite – gersdorffite and tennantite, and both are expected to report to the Cu concentrate (Fuerstenau et al., 2007). Smelters can normally only treat copper concentrates in which the arsenic level is $<$0.5 wt% and a penalty of $3 USD/kg arsenic is charged for an arsenic concentration over 0.2 wt% (Nazari et al., 2017). The highest bulk As content measured in our samples was 120 μg/g. By using the deportment results from this study and Cu concentrate recovery data (KGHM Technical Report, 2013), a feed at this level would yield a theoretical Cu concentrate containing ~0.15–0.2 wt% As. This is consistent with the grade of the concentrate fed to the Legnica smelter (0.2 wt% As; KGHM Technical Report, 2013). Although this predicted As content remains below the penalty threshold, it will be important for an eventual mineral processing operation to monitor As concentrations in the feed material in order to assure that the penalty threshold will not be exceeded. This may require careful blending of ores from different parts of the orebody.

With the exception of one sample from the T1 unit (sample 131–4; 12 μg/g), the bulk concentration of Bi in the ore was found to be rather uniform and low (below 1 μg/g). Based on the elemental deportment from the T1 samples and Cu concentrate recovery data (KGHM Technical Report, 2013), the average Bi content of a theoretical Cu concentrate is not expected to breach 45 μg/g and thus remain well below the typical smelter penalty threshold of 200 μg/g. This aligns with a Bi grade of 7 μg/g reported from the Cu concentrate fed to the Legnica smelter (KGHM Technical Report, 2013). Consequently, Bi is unlikely to present a metallurgical or environmental concern.

6. Conclusion

This investigation into the distribution of Co, Ni, As, and Bi in ores from the Spremberg-Graustein-Schleife prospect in Lusatia highlights the complex mineralogical and geochemical distribution of these minor elements in Kupferschiefer-type mineralization. Cobalt, Ni, and As occur in a variety of host minerals whose importance varies across different mineralization zones. In the Cu zone, discrete Co, Ni, and As minerals occur as the main recoverable hosts of these metals. Members of the cobaltite – gersdorffite solid solution series are particularly abundant at the base of the T1 (carbonaceous shale) unit and along its contact with the underlying S1 (sandstone) unit.

Since Co, Ni, and As minerals predominantly occur as fine inclusions within the ore-forming Cu(Fe)-sulfides, they will almost certainly report to the Cu- and Ag-rich flotation concentrate. Other Co, Ni, and As minerals that are not directly associated with Cu(Fe)-sulfides may also be recovered, owing to their similar response to flotation reagents (Fuerstenau et al., 2007). In the Pb-Zn zone, pyrite represents the principal host of Co, Ni, and As. This type of mineralization is currently subeconomic and thus not exploited. However, if economic circumstances change, it is likely that Co- and Ni-bearing pyrite would be recovered together with galena (main Pb ore mineral) and sphalerite (main Zn ore mineral). Arsenic shows a similar behavior to Co and Ni; it occurs either as fine inclusions within Cu-sulfides or as As-bearing minerals that may be recovered together with the Cu-sulfide ore minerals. If present in high concentrations, this may actually cause smelter penalties. Bismuth is generally incorporated into ore-forming Cu(Fe)-sulfides. Its concentration is, however, very low in the ore and thus unlikely to incur smelter penalties.

CRediT authorship contribution statement

Zahra Nourizenouz: Writing – review & editing, Writing – original draft, Visualization, Validation, Methodology, Investigation, Formal analysis, Data curation, Conceptualization. **Max Frenzel:** Writing – review & editing, Supervision, Resources, Project administration, Funding acquisition, Conceptualization. **Bradley Martin Guy:** Writing – review & editing, Validation, Formal analysis, Conceptualization. **Aratz Beranoaguirre:** Writing – review & editing, Formal analysis. **Jens Gutzmer:** Writing – review & editing, Supervision, Resources, Project administration, Funding acquisition, Conceptualization.

Declaration of competing interest

The authors declare the following financial interests/personal relationships which may be considered as potential competing interests:

Jens Gutzmer reports financial support was provided by KSL Kupferschiefer Lausitz GmbH. If there are other authors, they declare that they have no known competing financial interests or personal relationships that could have appeared to influence the work reported in this paper.

Acknowledgments

This work was funded by KSL Kupferschiefer Lausitz GmbH (Spremberg, Germany). We thank Mr. Ralph Braumann and Mr. Blas Urioste of KSL for their generous support. We also gratefully acknowledge Dr. Joachim Krause (HIF) for help with EPMA data acquisition and processing. Finally, we gratefully acknowledge the technical support of Roland Wuerkert and Michael Stoll (both HIF) for preparation of polished sample sections and grain mounts. In addition, we would like to thank the editors, Dr. Martiya Sadeghi and two anonymous reviewers for their helpful and constructive comments that helped us to improve this manuscript.

Appendix A. Supplementary data

Supplementary data to this article can be found online at https://doi.org/10.1016/j.gexplo.2026.108060.

Data availability

All data used in this study are provided in the supplementary materials.

References

Actlabs, 2023. Multi-method analysis. https://actlabs.com/geochemistry/exploration-geochemistry/multi-method-analysis/ (Accessed June 2023).

Banas, M., Kijewski, P., Salamon, W., 1996. Accompanying metals in the copper ore deposit (in Polish). In: KGHM Polska Miedź S.A. Monograph, Lubin, pp. 258–271.

Borg, G., Piestrzyński, A., Bachmann, G.H., Püttmann, W., Walther, S., Fiedler, M., 2012. An overview of the European Kupferschiefer deposits. In: Hedenquist, J.W., Harris, M., Camus, F. (Eds.), Geology and Genesis of Major Copper Deposits and Districts of the World: A Tribute to Richard H. Sillitoe, 16. Soc. Econ. Geol., Special Publication, pp. 455–486.

Butcher, A.R., Helms, T., Gottlieb, P., 2000. Advances in the quantification of gold deportment by QEMSCAN. In: In: Proceedings of the Seventh Mill Operators' Conference, Kalgoorlie, Western Australia. AusIMM, Melbourne, pp. 267–271.

Cabri, L.J., Martin, C.J., Nelson, M., 2009. Deportment methodology for low-grade Ni-Cu-PGE ores. In: Proceedings of the Conference of Metallurgists, Sudbury, Canada. Canadian Institute of Mining, Metallurgy and Petroleum.

Chryssoulis, S.L., Cabri, L.J., 1990. Significance of gold mineralogical balance in mineral processing. Trans. Inst. Min. Metall. A 99, C1–C10.

Coetzee, L.L., Theron, S.J., Martin, G.J., et al., 2011. Modern gold deportments and its application to industry. Miner. Eng. 24, 565–575. https://doi.org/10.1016/j.mineng.2010.09.001.

Cook, N.J., Ciobanu, C.L., Danyushevsky, L.V., Gilbert, S., 2011. Minor and trace elements in bornite and associated Cu–(Fe)-sulfides: a LA-ICP-MS study. Geochim. Cosmochim. Acta 75, 6473–6496. https://doi.org/10.1016/j.gca.2011.08.021.

Dehaine, Q., Tijsseling, L., Glass, H.J., Törmänen, T., Butcher, A.R., 2021. Geometallurgy of cobalt ores: a review. Miner. Eng. 160, 106656. https://doi.org/10.1016/j.mineng.2020.106656.

Duscher, G., Chisholm, M., Alber, U., et al., 2004. Bismuth-induced embrittlement of copper grain boundaries. Nat. Mater. 3, 621–626. https://doi.org/10.1038/nmat1191.

European Commission, 2023. Study on the critical raw materials for the EU 2023 – Final report. Publications Office of the European Union, Luxembourg. https://doi.org/10.2873/725585. Available at.

Fandrich, R., Gu, Y., Burrows, D., Moeller, K., 2007. Modern SEM-based mineral liberation analysis. Int. J. Miner. Process. 84, 310–320. https://doi.org/10.1016/j.minpro.2006.07.018.

Foltyn, K., Bertrandsson Erlandsson, V., Zygo, W., Melcher, F., Pieczonka, J., 2022. New perspective on trace element (Re, Ge, Ag) hosts in the Cu-Ag Kupferschiefer deposit, Poland: insight from a LA-ICP-MS trace element study. Ore Geol. Rev. 143, 104768. https://doi.org/10.1016/j.oregeorev.2022.104768.

Fountain, C., 2013. The whys and wherefores of penalty elements in copper concentrates. In: MetPlant 2013: Metallurgical Plant Design and Operating Strategies, Perth, WA, Australia, 15–17 July 2013. AusIMM, Carlton, VIC, pp. 1–10.

Frenzel, M., Tolosana-Delgado, R., Gutzmer, J., 2015. Assessing the supply potential of high-tech metals – A general method. Res. Policy 46 (2), 45–58. https://doi.org/10.1016/j.resourpol.2015.08.002.

Frenzel, M., Mikolajczak, C., Reuter, M.A., Gutzmer, J., 2017. Quantifying the relative availability of high-tech by-product metals – The cases of gallium, germanium and indium. Res. Policy 52, 327–335. https://doi.org/10.1016/j.resourpol.2017.04.008.

Frenzel, M., Bachmann, K., Carvalho, J.R.S., et al., 2019. The geometallurgical assessment of by-products—geochemical proxies for the complex mineralogical deportment of indium at Neves-Corvo, Portugal. Mineral. Deposita 54, 959–982. https://doi.org/10.1007/s00126-018-0849-6.

Fuerstenau, M.C., Chander, S., Woods, R., 2007. Sulfide mineral flotation. In: Fuerstenau, M.C., Jameson, G.J., Yoon, R.H. (Eds.), Froth Flotation: A Century of Innovation. Society for Mining, Metallurgy, and Exploration (SME), Littleton, Colorado, pp. 425–464.

Geißler, M., Breitkreuz, C., Kiersnowski, H., 2008. Late Paleozoic volcanism in the central part of the Southern Permian Basin (NE Germany, W Poland): facies distribution and volcano-topographic hiati. Int. J. Earth Sci. 97, 973–989. https://doi.org/10.1007/s00531-007-0288-6.

Glennie, K.W., 1997. Recent advances in understanding the southern North Sea Basin: a summary. Geol. Soc. Lond. Spec. Publ. 123, 17–29. https://doi.org/10.1144/gsl.sp.1997.123.01.03.

Goodall, W.R., 2008. Characterisation of mineralogy and gold deportment for complex tailings deposits using QEMSCAN®. Miner. Eng. 21, 518–523. https://doi.org/10.1016/j.mineng.2008.02.022.

Goodall, W.R., Scales, P.J., Butcher, A.R., 2005. The use of QEMSCAN and diagnostic leaching in the mineralization of visible gold in complex ores. Miner. Eng. 18, 877–886. https://doi.org/10.1016/j.mineng.2005.01.018.

Greffe, T., Frenzel, M., Werner, T.T., et al., 2024. Byproduct-to-host ratios for assessing the accessibility of mineral resources. Environ. Sci. Technol. 58, 22213–22223. https://doi.org/10.1021/acs.est.4c05293.

Gregory, D.D., Large, R.R., Halpin, J.A., et al., 2015. Trace element content of sedimentary pyrite in black shales. Econ. Geol. 110, 1389–1410. https://doi.org/10.2113/econgeo.110.6.1389.

Gu, Y., 2003. Automated scanning electron microscope based mineral liberation analysis: an introduction to JKMRC/FEI mineral liberation analyser. J. Miner. Mater. Charact. Eng. 2, 33–41. https://doi.org/10.4236/jmmce.2003.21003.

Heinig, T., Bachmann, K., Tolosana-Delgado, R., van den Boogaart, G., Gutzmer, J., 2015. Monitoring gravitational and particle shape settling effects on MLA sampling preparation. In: In: Proceedings of the 18th Annual IAMG Conference, Freiberg. IAMG, Houston, pp. 200–206.

Hitzman, M., Kirkham, R., Broughton, D., et al., 2005. The sediment-hosted stratiform copper ore system. In: Hedenquist, J.W., Thompson, J.F.H., Goldfarb, R.J., Richards, J.P. (Eds.), One Hundredth Anniversary Volume. Society of Economic Geologists.

IEA, 2024. Global Critical Minerals Outlook 2024. International Energy Agency, Paris.

Jochum, K.P., Weis, U., Stoll, B., Kuzmin, D., Yang, Q., Raczek, I., Jacob, D.E., Stracke, A., Birbaum, K., Frick, D.A., Günther, D., Enzweiler, J., 2011. Determination of reference values for NIST SRM 610–617 glasses following ISO guidelines. Geostand. Geoanal. Res. 35. https://doi.org/10.1111/j.1751-908X.2011.00120.x.

Kaiser, R., Nöth, S., Ricken, W., 2003. Sequence stratigraphy with emphasis on platform-related parasequences of the Zechstein 2 carbonate (Ca2) – the northern platform margin of the Southern Permian Basin (NE Germany). Int. J. Earth Sci. 92, 54–67. https://doi.org/10.1007/s00531-002-0292-9.

Kelvin, M., Whiteman, E., Petrus, J., Leybourne, M., Nkuna, V., 2022. Application of LA-ICP-MS to process mineralogy: gallium and germanium recovery at Kipushi copper-zinc deposit. Miner. Eng. 176, 107322. https://doi.org/10.1016/j.mineng.2021.107322.

KGHM Technical Report, 2013. "Technical Report on the Copper-Silver Production Operations of KGHM Polska Miedź S.A. in the Legnica-Głogów Copper Belt Area of Southwestern Poland" prepared by Micon International Limited. https://kghm.com/en/technical-report-copper-silver-production-operations-kghm-polska-miedz-sa-legnica-glogow-copper.

KGHMa, 2025. Metals produced. https://kghm.com/en/our-business/products (accessed October 2025).

KGHMb, 2025. Smelting and refining. https://kghm.com/en/our-business/smelting-and-refining (accessed October 2025).

Kim, Y., Frenzel, M., Guy, B.M., Thiele, S.T., Braumann, R., Gutzmer, J., 2024. Development of New Exploration Vectors by Quantitative Mineralogical Analysis at the Spremberg-Graustein-Schleife Cu-Ag Kupferschiefer Deposit, Lusatia, Germany. In: SEG 2024 Conference: Sustainable Mineral Exploration and Development, Windhoek, Namibia.

Klette, W., 2003. Die komplexe Nutzung der Wertkomponenten aus dem Mansfelder Kupferschiefer – bergbauliche Nutzung und Verwahrung. Anschnitt 3–5, 148–159.

Kopp, J.C., 2022. Kupfer-silber-Lagerstätten im basalen Zechstein (Oberes Perm) zwischen Leszczyńa (Nordsudetische Mulde, Polen) und Spremberg (Lausitz, Deutschland). Schriftenr. Dtsch. Ges. Geowiss. 97.

Kopp, J.C., Simon, A., Göthel, M., 2006. Die Kupfer-Lagerstätte Spremberg-Graustein in Südbrandenburg. Brandenburg. Geowiss. Beitr. 13, 117–132.

Kopp, J.C., Spieth, V., Höding, T., 2010. Revival of copper mining in Germany. Glückauf-Mining-Reporter 2, 43–53.

Kopp, J.C., Spieth, V., Bernhardt, H., 2012. Precious metals and selenides mineralisation in the copper silver deposit Spremberg-Graustein, Niederlausitz, SE Germany. Z. Dtsch. Ges. Geowiss. 163 (4), 361–384.

KSL Internal Report, 2021.

Kucha, H., 1990. Geochemistry of the Kupferschiefer, Poland. Geol. Rundsch. 79, 387–399. https://doi.org/10.1007/BF01830634.

Kucha, H., Pawlikowski, M., 1986. Two-brine model of the genesis of strata-bound Zechstein deposits (Kupferschiefer type), Poland. Mineral. Deposita 21, 70–80. https://doi.org/10.1007/BF00204365.

Large, D.J., Sawłowicz, Z., Spratt, J., 1999. A cobaltite-framboidal pyrite association from the Kupferschiefer: possible implications for trace element behaviour during the earliest stages of diagenesis. Mineral. Mag. 63 (3), 353–361. https://doi.org/10.1180/002646199548574.

Long, G., Peng, Y., Bradshaw, D., 2012. A review of copper–arsenic mineral removal from copper concentrates. Miner. Eng. 36–38, 179–186. https://doi.org/10.1016/j.mineng.2012.03.032.

Mikulski, S.Z., 2022. Cobalt potential from the metallic deposits in Poland. In: In: 16th SGA Biennial Meeting, Rotorua.

Moats, M.S., Davenport, W.G., 2014. Nickel and cobalt production. In: Seetharaman, S. (Ed.), Treatise on Process Metallurgy. Elsevier, pp. 625–669. https://doi.org/10.1016/B978-0-08-096988-6.00026-2.

Mudd, G.M., Jowitt, S.M., Werner, T.T., 2017. The world's by-product and critical metal resources part I: Uncertainties, current reporting practices, implications and grounds for optimism. Ore Geol. Rev. 86, 924–938. https://doi.org/10.1016/j.oregeorev.2016.05.001.

Nassar, N.T., Graedel, T.E., Harper, E.M., 2015. By-product metals are technologically essential but have problematic supply. Sci. Adv. 1, e1400180. https://doi.org/10.1126/sciadv.1400180.

Nazari, A.M., Radzinski, R., Ghahreman, A., 2017. Review of arsenic metallurgy: Treatment of arsenical minerals and the immobilization of arsenic. Hydrometallurgy 174, 258–281. https://doi.org/10.1016/j.hydromet.2016.10.011.

Nourizenouz, Z., Guy, B.M., Gutzmer, J., Ebert, D., Braumann, D., Frenzel, M., 2026. The deportment of silver in Kupferschiefer ores at the Spremberg-Graustein-Schleife deposit, Germany. Mineral. Deposita 61, 67–89. https://doi.org/10.1007/s00126-025-01377-5.

Onuk, P., Melcher, F., Mertz-Kraus, R.G., Abler, H.E., Goldmann, S., 2017. Development of a matrix-matched sphalerite reference material (MUL-ZnS-1) for calibration of in situ trace element measurements by laser ablation-inductively coupled plasma-mass spectrometry. Geostand. Geoanal. Res. 41, 263–272. https://doi.org/10.1111/ggr.12154.

Piestrzyński, A., Pieczonka, J., Głuszek, A., 2002. Redbed-type gold mineralization, Kupferschiefer, south-west Poland. Mineral. Deposita 37, 512–528. https://doi.org/10.1007/s00126-001-0230-5.

Rahfeld, A., Gutzmer, J., 2017. MLA-based detection of organic matter with iodized epoxy resin—an alternative to carnauba. J. Miner. Mater. Charact. Eng. 5, 198–208. https://doi.org/10.4236/jmmce.2017.54017.

Savard, D., Bouchard-Boivin, B., Barnes, S.J., Garbe-Schönberg, D., 2018. UQAC-FeS: A new series of base metal sulfide quality control reference material for LA-ICP-MS

analysis. In: In: Proceedings of the 10th International Conference on the Analysis of Geological and Environmental Materials, Sydney, Australia, pp. 8–13.
Sawłowicz, Z., 1985. Significance of metalloporphyrins for the metal accumulation in the copper-bearing shales from the Zechstein copper deposits (Poland). Mineral. Pol. 16, 35–42.
Slack, J.F., Kimball, B.E., Shedd, K.B., 2017. Critical mineral resources of the United States—Economic and environmental geology and prospects for future supply, 1802. U.S. Geol. Surv. Prof. Pap., pp. F1–F40. https://doi.org/10.3133/pp1802F. Cobalt, chap. F of Schulz, K.J., DeYoung, J.H., Jr., Seal, R.R., II, and Bradley, D.C., eds.
Spilker, M., 2010. 800 years of copper shale mining in the southern Harz. In: Proceedings of the 12th South Harz Symposium, 6 March 2010, Wettelrode, Mansfeld-South Harz District.
Stodulski, M., Drzymala, J., 2016. Flotation of copper-bearing carbonaceous shale in the presence of amine type frothers. Ann. Univ. Mariae Curie-Sklodowska 71, 69–78. https://doi.org/10.17951/aa.2016.71.1.69.
Stollhofen, H., Bachmann, G.H., Barnasch, J., Bayer, U., Beutler, G., Franz, M., Kästner, M., Legler, B., Mutterlose, J., Radies, D., 2008. Upper Rotliegend to Early Cretaceous basin development. In: Littke, R., Bayer, U., Gajewski, D., Nelskamp, S. (Eds.), Dynamics of complex intracontinental basins. Springer-Verlag, Berlin, Heidelberg, pp. 181–210.
Strohmenger, C., Voigt, E., Zimdars, J., 1996. Sequence stratigraphy and cyclic development of Basal Zechstein carbonate-evaporite deposits with emphasis on Zechstein 2 off-platform carbonates (Upper Permian, Northeast Germany). Sediment. Geol. 102, 33–54. https://doi.org/10.1016/0037-0738(95)00058-5.
Tucker, M.E., 1991. Sequence stratigraphy of carbonate-evaporite basins: Models and application to the Upper Permian (Zechstein) of northeast England and adjoining North Sea. J. Geol. Soc. Lond. 148, 1019–1036. https://doi.org/10.1144/gsjgs.148.6.1019.
U.S. Department of Energy, 2023. Critical Materials Assessment. U.S. Department of Energy, Washington, DC. https://www.energy.gov/eere/ammto/articles/2023-doe-critical-materials-assessment.
Van Wees, J.-D., Stephenson, R.A., Ziegler, P.A., et al., 2000. On the origin of the Southern Permian Basin, Central Europe. Mar. Pet. Geol. 17, 43–59. https://doi.org/10.1016/S0264-8172(99)00052-5.
Vind, J., Tamm, K., 2021. Review of the extraction of key metallic values from black shales in relation to their geological and mineralogical properties. Miner. Eng. 174, 107271. https://doi.org/10.1016/j.mineng.2021.107271.
Wagner, T., Lorenz, J., 2002. Mineralogy of complex Co-Ni-Bi vein mineralization, Bieber deposit, Spessart, Germany. Mineral. Mag. 66, 385–407. https://doi.org/10.1180/0026461026630036.
Wilson, S.A., Ridley, W.I., Koenig, A.E., 2002. Development of sulfide calibration standards for the laser ablation inductively coupled plasma mass spectrometry technique. J. Anal. At. Spectrom. 17, 406–409. https://doi.org/10.1039/B108787H.
Zhang, Y., Fan, Y., Liu, Y., Zhou, T., Ou, B., 2024. Distribution and enrichment processes of cobalt in the Longqiao iron skarn deposit in Eastern China. Ore Geol. Rev. 174, 106277. https://doi.org/10.1016/j.oregeorev.2024.106277.
Ziegler, P.A., 1990. Geological Atlas of Western and Central Europe, second ed. Shell Internationale Petroleum Maatschappij B.V. and Geological Society, London.